Manuel Wurzer, Bsc.

# Machine Learning for Predicting Time Temperature Transformation in Bainitic Steel

**Master's Thesis**
to achieve the university degree of
Master of Science
Master's degree programme: Information and Computer Engineering

submitted to

**Graz University of Technology**

Supervisors
Franz Pernkopf
Sophie Steger

Signal Processing and Speech Communication Laboratory

Graz, May 2024

# Affidavit

I declare that I have authored this thesis independently, that I have not used other than the declared sources/resources, and that I have explicitly indicated all material which has been quoted either literally or by content from the sources used. The text document uploaded to TUGRAZonline is identical to the present master's thesis.

10.06.2024

Date Signature

# Eidesstattliche Erklärung

Ich erkläre an Eides statt, dass ich die vorliegende Arbeit selbstständig verfasst, andere als die angegebenen Quellen/Hilfsmittel nicht benutzt, und die den benutzten Quellen wörtlich und inhaltlich entnommenen Stellen als solche kenntlich gemacht habe. Das in TUGRAZonline hochgeladene Textdokument ist mit der vorliegenden Masterarbeit identisch.

10.06.2024

Datum

Unterschrift

# Abstract

In steel industry different alloys and heat treatments are used to create materials which fulfil certain properties. A combination of high strength and good ductility is a desired property and can be found in carbide-free bainitic (CFB) steel. The heat treatment allowing the microstructure of CFB steels to form can take up to days, which is not suitable for industry use. Therefore the transformation time expressed in the Time-Temperature-Transformation (TTT) is of great importance to analyse the behaviour of steel alloys during heat treatment. However, the determination of the TTT is expensive and takes a lot of time. This process requires precise measurement of the dilatation of specimens at various temperatures. Past research has used Machine Learning (ML) approaches and physical models to predict the behaviour of the whole TTT. This is mostly done by dividing the TTT into smaller subproblems. These subproblems result from the inherent complexity of the TTT and cover microstructures like martensite, ferrite and bainite. We specifically target predicting TTT for CFB steels, by using a dataset of 56 different material compositions. Random Forests (RFs) and Gaussian Process Regressors (GPRs) are used to predict transformation times. GPRs provide a measure for uncertainty additional to its predictions, which can give insights about how confident the ML model predicts the transformation times. The RF is used because of fast training behaviour and simple hyperparameter tuning. Furthermore, both models allow insight into the significance of specific input features. The feature importance from the RF or the trained length-scales from the GPR are used to determine which input features are important for the model's predictions. The findings of the thesis indicate that, for most predictions, the models are sufficiently accurate. However, the sparsity of the data prevents the model from being precise in certain areas of the feature input space, particularly for certain alloys. Both the GPR and the RF approach have significant potential to allow finding suitable CFB steels with short transformation times. Further research and the creation of a more comprehensive database of measurements will enhance the prediction performance.

# Kurzfassung

In der Stahlindustrie werden verschiedene Legierungen und Wärmebehandlungen verwendet, um Materialien mit bestimmten Eigenschaften herzustellen. Eine Kombination aus hoher Festigkeit und guter Duktilität ist eine erwünschte Eigenschaft und kann in karbidfreiem bainitischem (CFB) Stahl gefunden werden. Die Wärmebehandlung, die es der Mikrostruktur von CFB-Stählen ermöglicht, sich zu bilden, kann mehrere Tage dauern, was für den industriellen Einsatz nicht geeignet ist. Daher ist die Bestimmung der Transformationszeit, ausgedrückt in der Zeit-Temperatur-Umwandlungs (TTT)-Kurve, von großer Bedeutung für die Analyse des Verhaltens von Stahllegierungen während der Wärmebehandlung. Die Bestimmung der TTT ist jedoch teuer und zeitaufwendig. Dieser Prozess erfordert präzise Messungen der Dilatation von Proben bei verschiedenen Temperaturen. In der Vergangenheit wurden ML-Ansätze und physikalische Modelle verwendet, um das Verhalten der gesamten TTT vorherzusagen. Dies wird hauptsächlich durch die Unterteilung der TTT in kleinere Teilprobleme erreicht. Diese Teilprobleme resultieren aus der inhärenten Komplexität der TTT und umfassen Mikrostrukturen wie Martensit, Ferrit und Bainit. Wir zielen speziell darauf ab, die TTT für CFB Stahl vorherzusagen, indem wir einen Datensatz von 56 verschiedenen Materialzusammensetzungen verwenden. Random Forests (RF) und Gauß-Prozess-Regressoren (GPR) werden verwendet, um die Transformationszeiten vorherzusagen. GPRs bieten zusätzlich zu ihren Vorhersagen ein Maß an Unsicherheit, das Aufschluss darüber geben kann, wie zuversichtlich das ML-Modell die Transformationszeiten vorhersagt. Der RF wird aufgrund seines schnellen Trainingsverhaltens und der einfachen Hyperparameterabstimmung verwendet. Darüber hinaus geben beide Modelle Information wie wichtig bestimmte Input Features sind. Die sogenannte Featureimportance des RF oder die trainierten lenght-scale Parameter des GPR werden verwendet, um zu bestimmen, welche Input Features für die Vorhersagen des Modells wichtig sind. Die Ergebnisse der Arbeit zeigen, dass die Modelle für die meisten Schätzungen hinreichend genau sind. Der nicht ausreichende Datensatz verhindert jedoch, dass das Modell in bestimmten Bereichen (z.B. verschiedener Temperaturen) nicht präzise ist. Sowohl der GPR- als auch der RF-Ansatz haben erhebliches Potenzial, um geeignete CFB-Stähle mit kurzen Transformationszeiten zu finden. Weitere Forschung und die Erstellung einer umfassenderen Datenbank von Messungen werden die Vorhersageleistung verbessern.

# Acknowledgment

I would like to thank Franz Pernkopf for giving me the opportunity to work on this interesting topic and for his continuous support and valuable input. Furthermore, I thank Sophie Steger for further supervision throughout the thesis and Bernd Schuscha, who provided the data and found the time to join our regular meetings and guiding us through the field of material science, in particular the TTT diagrams. Last but not least, I want to thank my family and friends for always being there and supporting me during my journey to get my master's degree.

# Contents

# List of Figures

# List of Tables

# List of Acronyms and Abbreviations

**GP** Gaussian Process

**GPR** Gaussian Process Regressor

**RF** Random Forest

**NN** Neural Network

**TTT** Time Temperature Transformation

**MCL** Material Center Leoben

**CTE** Coefficient of Thermal Expansion

**ML** Machine Learning

**MAPE** Mean Absolute Percentage Error

**CFB** Carbide-Free Bainitic

# 1 Introduction

The development of novel steel alloys with tailored properties plays a vital role across various industries, including aerospace, automotive, construction and infrastructure. This thesis focuses on Carbide-free bainitic (CFB) steel which can have high strength and high ductility. Certain alloys combined with a different type of heat treatment forms the desired microstructure within the steel. However, the heat treatment used to transform the microstructure can take up to days, which makes the use of such alloys not suitable for the industry. The goal is to help find alloys which form CFB steels with a short transformation time during heat treatment using only data driven ML models. Traditionally, engineers have relied on dilatometry experiments to create Time-Temperature-Transformation (TTT) diagrams. TTT behaviour of certain steels are used to summarize and analyse the behaviour of steels during heat treatment within different microstructures. However, these experiments are time-consuming, expensive and are therefore limited in their ability to capture the full spectrum of potential steel compositions.

### Scope

This thesis examines the potential of non-parametric Machine Learning (ML) models to learn complex, non-linear relationships within the steels transformation without using prior assumptions about the underlying physical mechanisms. The conventional ML approach and the approach also taken in this thesis is to split the TTT into subproblems. Each subproblem covers one microstructure of steel. The focus in this thesis lies on the microstructure of CFB steels and their transformation behaviour during heating, rapid cooling and further maintaining a constant temperature. Focusing on CFB steels does not necessarily exclude the possibility of applying established ML models to other microstructures, like ferrite, for instance. Due to their advantages especially for this use case the ML models tested and implemented are Random Forest (RF) and the Gaussian Process Regressors (GPR). One advantage is, that GPRs allow uncertainty estimates in addition to the targets predictions, providing information about how trustworthy prediction are. This is important, because the insufficient size of the available data set does not always allow confident predictions. The RF is used due to its fast training behaviour and straightforward hyperparameter tuning. Both ML models allow an insight into which input features are particularly of interest, by analysing the feature importance

of the RF and the length-scale parameters of the GPR. The quality of the data in terms of the measurement errors is of importance to ensure a good prediction performance. The provided data encompasses direct measurements obtained through dilatometry experiments which were conducted by the Material Center Leoben (MCL) and measurements gathered from scientific publications. The application of ML models has the potential to significantly reduce the time and resources required to generate TTT diagrams compared to conducting multiple dilatometry experiments. This will further help find CFB steels with a short transformation time. Training of models on more comprehensive datasets will improve the accuracy of TTT diagram predictions.

### Outlook

The remainder of this thesis is structured as follows:

Chapter 2 delves into the fundamentals of TTT diagrams, the principles of dilatometry, and critically reviews existing literature on related research efforts in this field.

Chapter 3 gives a brief overview to ML and the specific models used, such as RF and GPR.

Chapter 4 introduces the methodology of regression of TTT, including a detailed description of the challenges and how the data is structured.

Chapter 5 presents the results obtained from applying GPR and RF to the prepared data followed by a comprehensive evaluation of their performance and predictive capabilities. Furthermore, limitations are discussed.

Finally, Chapter 6 draws key conclusions from the results and outlines recommendations for future work.

# 2 Background and Related Work

## 2.1 Dilatometry

Information of the data generating process is an advantage when it comes to analysing the data. Therefore, an introduction into the dilatometry experiment is given in this section.

Heating or cooling various materials causes them to expand or contract. This thermal expansion is used to gain information about the material transformations. Every substance reacts differently to temperature changes. This can be expressed and measured with the Coefficient of Thermal Expansion (CTE). The higher the coefficient, the more an element expands while being heated. The CTE can also be negative. A negative coefficient means, that the specimen contracts while being heated. In a dilatometry experiment this expansion and contraction of a substance is measured. The point is to show the lengthening of the material relative to the temperature. These positive and negative CTE are single-phase characteristics that result from a continuous change in the temperature (Hunkel et al., 2018).

In a steel alloy of different compounds, this dilation is not straightforward. It is possible to have continuities in the volume temperature curve due to the transformation of the microstructure within the steel alloy. Additionally, the presence of different elements within the alloy can induce stress, as they expand or contract at varying rates for different temperature changes. Phase transitions such as the ferro- to paramagnetic transition exhibit a continuous volume change but a discontinuity in the CTE. This characteristic makes them detectable through dilatometry due to the abrupt changes in volume or its derivative. Phase transformations, on the other hand, involve a shift in the lattice structure, like the transition from body-centered cubic to face-centered cubic seen in the transformation of iron from ferrite to austenite, for instance. This lattice alteration results in an additional length change, superimposed on thermal expansion, which can be either positive or negative depending on the packing density of the parent and daughter phases (Hunkel et al., 2018).

Dilatometry offers the capability to not only analyse the expansion or contraction of alloyed steel but also to gather valuable information about phase transformations due to its continuous behaviour. There are various approaches to the dilatometric evaluation of phase transformation, one of which is the transformation during iso-thermal holding, where the temperature is held constant over a period of time.

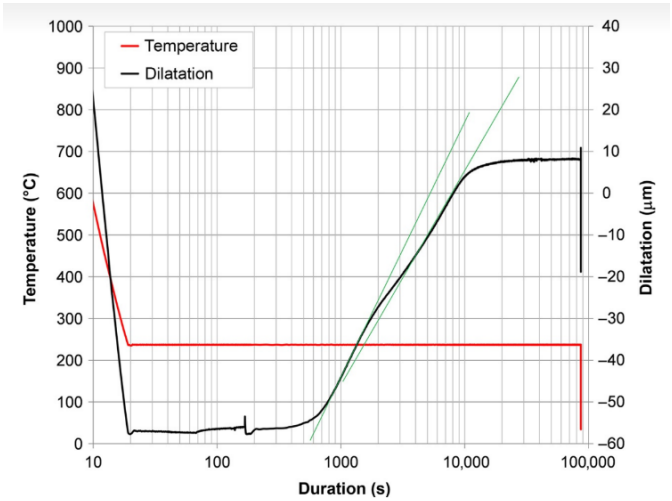


Figure 2.1: Measurement of the dilation of a certain alloy using iso-thermal holding, from Hunkel et al., 2018.

## 2.2 Time Temperature Transformation

Transformation during iso-thermal holding is the fundamental approach of interest within this thesis. During this approach, the specimen is heated up or cooled down to a certain temperature for which it will be held during the experiment (Hunkel et al., 2018). This can be seen in Figure 2.1.. The red line shows the temperature which was held constant at 237 °C right after cooling down the specimen from around 600 °C. The black line shows the dilation of the specimen. This graph summarizes the method used to collect the measurements for this thesis. The experiment reveals various kinematic phases, as denoted by the green lines. Initially, the expansion occurs rapidly, then slows down slightly in the middle phase before accelerating again.

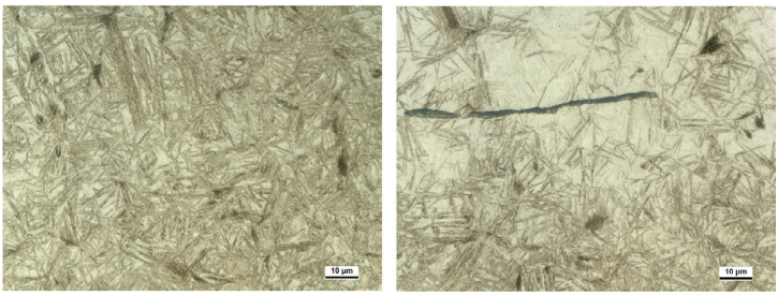

Figure 2.2: Transformation of bainitic steel during iso-thermal holding for 39 minutes, from Hunkel et al., 2018.

In Figure 2.2 the beginning and the end of the transformation can be seen. On the left side a tight bainite microstructure is shown, hence it is not expanded

yet. The right side shows how much the alloyed steel expanded throughout the experiment of iso-thermal holding.

The target property in this thesis is the bainitic phase fraction $f_B$, derived from the dilatometry experiment by using the "lever rule",

$$f_B = \frac{C - B}{C - A}. \tag{2.1}$$

where

- $A$: length of the specimen at the beginning of transformation.
- $B$: measured length of the specimen at time $t$.
- $C$: elongation of the specimen at complete transformation.

It compares the relative length difference with the volume fraction of the transformation. One method involves fitting the segments of the dilatometric curve before and after the phase transformation. The transformed phase fraction, seen in Figure 2.3, is evaluated based on the position of the measured dilatometric curve between the fitted lines (Yang et al., 2015).

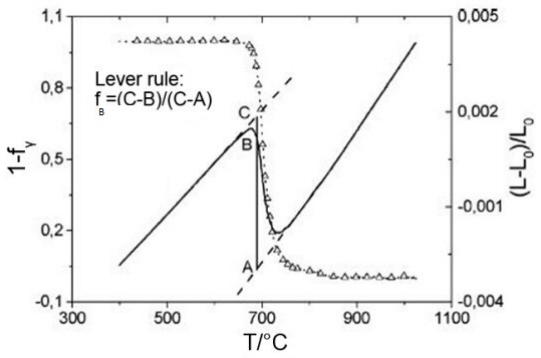


Figure 2.3: The lever rule in dilatometric analysis, from Yang et al., 2015.

Multiple measurements like this lead to the TTT diagram. Figure 2.4 shows the duration of the transformation over the iso-thermal temperature depending on the microstructure.

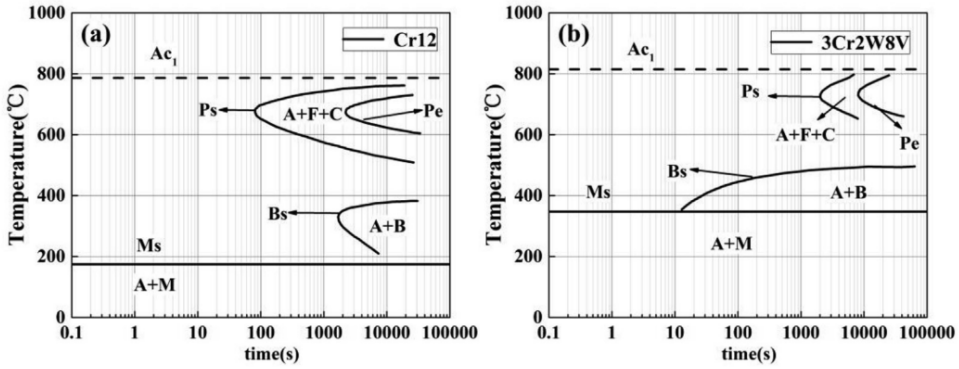


Figure 2.4: The TTT diagrams of high-alloy steels (a) Cr12; (b) 3Cr2W8V (A is Austenite; F is Ferrite; C is Cementite; B is Bainite; M is Martensite; Ac1 is the critical temperature of Austenite; Ms is the starting temperature of Martensite; Ps and Pe starting and end line of Pearlite transformation), from Huang et al., 2020.

As mentioned earlier, the conduction of all the experiments for getting sufficient data for the TTT is very time-consuming as well as very costly. Therefore, it is important for the industry to have good estimates for a certain alloy to meet the demand for material development. Numerous calculation methods based on empirical formulas exist, but they will not be extensively discussed in this thesis. Thermodynamics and kinetic models offer predictive capabilities for TTT diagrams. However, these methods have limitations as they often assume linear relationships among alloy elements within the composition (Huang et al., 2020). There is also software on the market which is commercially used. The software JMatPro uses the same linear relations as discussed. Improving predictions of TTT and surpassing current models will require an approach that incorporates non-linear models and multivariate analyses.

## 2.3 Bainite Microstrucutre

The TTT diagram encompasses all transformations and potential microstructures within the steel alloy, presenting a challenge for estimation. Typically, each mechanism must be predicted separately, effectively breaking down the problem into subproblems. In simpler terms, this means addressing each subproblem independently, which is the common approach in TTT diagram analysis. Current models are put together with submodels creating an estimate for every microstructure which then results in the TTT. This further simplifies the task in training models for each microstructure. Approaching the estimation by dividing it into subtasks sets the stage for the use-case of this thesis, which will focus on the bainite microstructure and its transformation within steel.

This sub-problem can be seen in Figure 2.4, where the part $A + B$ is of interest. This c-shape is the transformation of the alloys given with bainite steel. In the

right plot, only the upper half of the c-shape is seen, because on the lower part already another microstructure, martensite, takes over.

## 2.4 Data

In ML the data is of high importance. With sufficient and highly accurate data a highly accurate model can be trained. Faulty and noisy data can lead to loss in model performance and therefore wrong predictions. Reducing or avoiding possible measurement variances and outliers further improves the model. Because the experiment is not conducted as part of this work, there is no opportunity to influence the precision and accuracy of the given samples. However, pre-processing techniques can still be applied to improve the quality of the data. The given data originates from two distinct sources. One portion is measured by the Material Center Leoben (MCL), preprocessed, and then provided for this thesis. The other part is obtained from scientific papers, where it is interpreted and sampled from plots, rather than directly measured. This introduces additional error on top of the existing measurement error.

As discussed in Section 2.1 the data samples come from measuring the dilation over time. This is further expressed using the phase fraction $f_B$. The graphs for repeated measurements under the same conditions, material, and temperature, are shown in Figure 2.5. The plot provides insight into the variability of results from a single experiment, underscoring the presence of measurement errors. Three different measurements with the exact same setup reach 80% of $f_B$ at 29.4 seconds, 45.6 seconds and 55.2 seconds resulting in a difference of 27 seconds. Longer-lasting transformations tend to have larger absolute errors, while shorter measurements typically have smaller errors. The measurement accuracy further limits the prediction accuracy of the ML models.

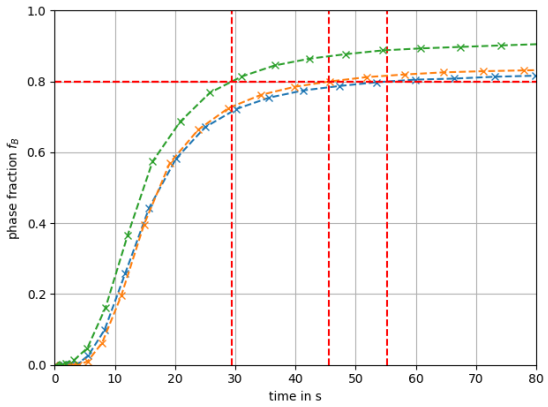


Figure 2.5: Multiple measurements of the same material at the same temperature (425°C) reaching the value $f_B = 0.8$ at different times resulting in a measurement error. The green line reaches $f_B = 0.8$ at 29.4, the orange at 45.6, and the blue at 55.2 seconds.

The data set comprises 56 materials. For each material, multiple experiments with different iso-thermal holding temperatures were conducted. Each measurement contains samples gathered from the dilatometry experiment. The information about the compound is provided for each material, by the vector $w_{per}$ which contains the weight percentage for each element.

Even for highly alloyed steels, iron (**Fe**) constitutes the most of the alloy composition. Other elements are added to achieve desired properties. The total percentage of all elements in the alloy composition sums up to 100%.

Figure 2.6 displays the 56 materials, illustrating the elements present in each alloy. Iron (**Fe**) is omitted from this plot since its presence in steel is assumed. Upon inspection of the plot, certain observations can be made. For instance, Boron (**B**) is the only element used just once among the alloys.

It is noteworthy that all materials contain Carbon (**C**), while the majority also include Silicon (**Si)**, Manganese (**Ma**), and Chromium (**Cr**). The influence of each element for the dilation measurement must be learned by the ML model.

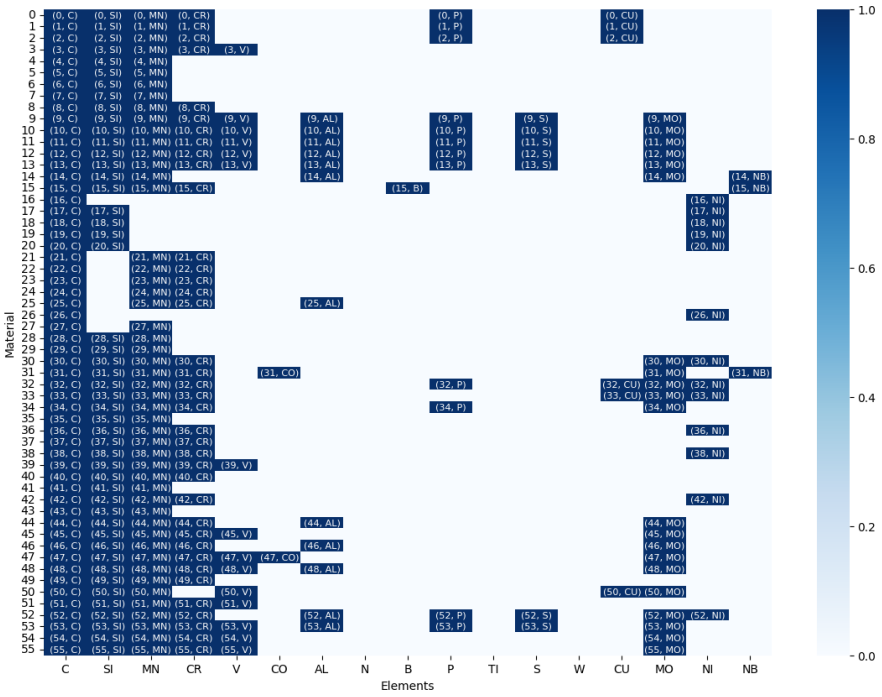


Figure 2.6: Material compositions: Dark blue indicates elements with a weight percentage above 0.

All chemical elements are carefully selected and combined to tailor the alloy's properties to specific requirements. Having various materials is a huge challenge for a ML model. Because small changes in the composition may cause high variance in the output. Underrepresented materials without similarity to other materials in the training data are difficult for the ML model to predict.

Additionally, to the weight percentage, the temperature at iso-thermal holding, $T_H$ in degrees Celsius, is given. This temperature is important as it acts as a driving force during the process of the transformation. There are one or more measurements per material, which lead to one or more iso-thermal holding temperatures given per material. As described in Section 2.1, this measurement is unique for one experiment.

# 3 Machine Learning Background

Machine learning is a subset of Artificial Intelligence that enables computers to learn from data and improve their performance on tasks without being explicitly programmed. It encompasses a variety of techniques and algorithms, broadly categorized into three main types: supervised learning, unsupervised learning and reinforcement learning.

Supervised learning involves training a model on a labelled dataset, where each example is paired with a corresponding target label. The model learns to map inputs to outputs by generalizing from the labelled data. It includes techniques such as: (i) Regression with the aim to predict continuous-valued outputs and (ii) Classification, where categorical labels are predicted.

Unsupervised learning deals with unlabelled data, where the model aims to discover patterns or structures inherent in the data without explicit guidance. It includes techniques such as: (i) Clustering with the aim to group similar data points and (ii), Dimensionality reduction, where reducing the number of features while preserving essential information is performed (iii), Reinforcement learning involves an agent learning to make decisions by interacting with an environment. The agent receives feedback in the form of rewards or penalties, allowing it to learn optimal strategies over time.

There are two different types of ML models: parametric and non-parametric models. Parametric models make assumptions about the functional form of the relationship between inputs and outputs and have a fixed number of parameters that are learned from the data. Examples include linear regression, logistic regression, and neural networks with a fixed architecture. Parametric models assume that there is a finite set of parameters $\theta$ describing the regression or the classification problem. The fixed set of parameters constraints the problem to a certain degree (Ghahramani, 2013). In parametric models, the future prediction $\hat{y}$ are independent of the observed data $\mathcal{D}$, i.e.

$$P(\hat{y}|\theta, \mathcal{D}) = P(\hat{y}|\theta). \tag{3.1}$$

Non-parametric models do not make strong assumptions about the underlying functional form. However, for predictions $\hat{y}$ data $\mathcal{D}$ is required. The

parameters $\theta$ of a non-parametric model typically grow in complexity with the size of the training data. One advantage of non-parametric models is, that, not as much data is required as for parametric models (Ghahramani, 2013).

Numerous models were implemented in this thesis. It turned out that the most successful ML approaches are RFs and GPRs. For this reason, the theory behind RFs and GPRs will be briefly outlined in the following section. Details about the use of these models is further discussed in Chapter 4.

## 3.1 Gaussian Process Regression

### Multivariate Gaussian

The Gaussian distribution is used to describe random variables. The combination of two or more random variables can be achieved using the multivariate Gaussian distribution, which can be further expressed using

$$p(\mathbf{x}|\boldsymbol{\mu}, \boldsymbol{\Sigma}) = \frac{1}{(2\pi)^{d/2}|\boldsymbol{\Sigma}|^{1/2}} \exp\left(-\frac{1}{2}(\mathbf{x}-\boldsymbol{\mu})^T\boldsymbol{\Sigma}^{-1}(\mathbf{x}-\boldsymbol{\mu})\right), \tag{3.2}$$

where

- $\mathbf{x} \in \mathbb{R}^d$ : Vector of random variables.
- $\boldsymbol{\mu} \in \mathbb{R}^d$: Mean vector.
- $\boldsymbol{\Sigma} \in \mathbb{R}^{d\times d}$: Covariance matrix.
- $|\boldsymbol{\Sigma}|$: The determinant of the covariance matrix.

In Figure 3.1, an example of a two-dimensional Gaussian distribution is depicted. This joint distribution effectively captures correlations between the input variables, illustrating the relationship between two random variables.

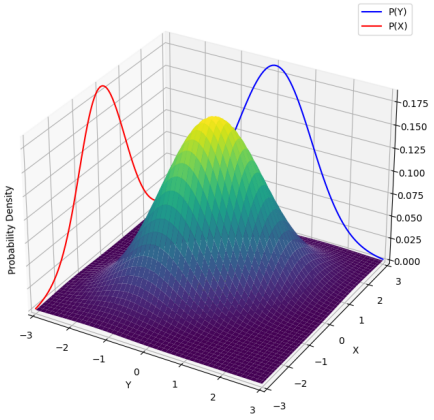


Figure 3.1: A multivariate Gaussian distribution of two input variables X and Y.

### Gaussian Processes

A stochastic process consists of an indexed collection of random variables. When these random variables are assumed to follow a Gaussian distribution, we obtain a Gaussian Process. The assumption of Gaussian distributed random variables simplifies the computational aspects of inference and learning.

The Gaussian process function can be described by the mean $m(\cdot)$ and covariance function $k(\cdot,\cdot)$ and is expressed as:

$$f(\cdot) \sim \mathcal{GP}\big(m(\cdot), k(\cdot,\cdot)\big). \tag{3.3}$$

The mean function represents the expected value of the target, while the covariance function describes the relationships between different input locations.

### Gaussian Process Regression

Assuming the real target values $\mathbf{f} = \begin{pmatrix} f_{\mathbf{x}_1} & \dots & f_{\mathbf{x}_n} \end{pmatrix}$ and the training samples $X = (\mathbf{x}_1, \dots, \mathbf{x}_n)$ are given. In the real world function values are not directly accessible, because a measurement is always subject to noise. The target values are therefore given as $\mathbf{y} = \mathbf{f} + \epsilon$, where the noise $\epsilon$ is independent identically distributed Gaussian noise with variance $\sigma_n^2$,

$$\epsilon \sim \mathcal{N}(0, \sigma_n^2). \tag{3.4}$$

The target is to estimate $\mathbf{f}_* = \begin{pmatrix} f_{\mathbf{x}_{*1}} & \dots & f_{\mathbf{x}_{*n}} \end{pmatrix}$ at the given test samples $X_* = (\mathbf{x}_{*1}, \dots, \mathbf{x}_{*n})$.

From the definition of the GP, it follows that,

$$\begin{bmatrix} \mathbf{y} \\ \mathbf{f}_* \end{bmatrix} \sim \mathcal{N}\left(\mathbf{0}, \begin{bmatrix} K(X,X) + \sigma_n^2 I & K(X,X_*) \\ K(X_*,X) & K(X_*,X_*) + \sigma_n^2 I \end{bmatrix}\right). \tag{3.5}$$

It is common to assume that the targets are drawn from a zero-mean prior Gaussian distribution. By using the calculation rules for multivariate normal distributions this can be used to make predictions on $\mathbf{f}_*$,

$$\begin{aligned} &\mathbf{f}_* | X, \mathbf{y}, X_* \sim \mathcal{N}\big(\bar{\mathbf{f}}_*, \operatorname{cov}(\mathbf{f}_*)\big), \text{where} \\ &\qquad \bar{\mathbf{f}}_* = \mathbb{E}[\mathbf{f}_* | X, \mathbf{y}, X_*] = K(X_*,X)[K(X,X) + \sigma_n^2 I]^{-1}\mathbf{y}, \\ &\operatorname{cov}(\mathbf{f}_*) = K(X_*,X_*) - K(X_*,X)[K(X,X) + \sigma_n^2 I]^{-1}K(X,X_*). \end{aligned} \tag{3.6}$$

The prediction of the target value is $\bar{\mathbf{f}}_*$ and the covariance matrix $\operatorname{cov}(\mathbf{f}_*)$ gives information about how certain the estimates are. In the case that there is only one test point $\mathbf{x}_*$ we write $\mathbf{k}(\mathbf{x}_*) = \mathbf{k}_*$ to denote the vector of covariances between the test point and the $n$ training points. Additionally the matrices of the covariances are written in the compact form of $K = K(X,X)$. For one test point $\mathbf{x}_*$ the equations are further written as,

$$\begin{aligned} \bar{f}_* &= \mathbf{k}_*^\top (K + \sigma_n^2 I)^{-1} \mathbf{y}, \\ \mathbb{V}[f_*] &= k(\mathbf{x}_*, \mathbf{x}_*) - \mathbf{k}_*^\top (K + \sigma_n^2 I)^{-1} \mathbf{k}_*, \end{aligned} \tag{3.7}$$

where $\mathbb{V}[f_*]$ denotes the variance of the prediction and $\bar{f}_*$ is the actual prediction value.

### Hyper-Parameter Learning

Regression problems often use the Radial Basis Function (RBF) kernel. The kernel is calculated as follows,

$$k_{SE}(x, x') = \exp\left(-\frac{1}{2\tau^2}||x - x'||^2\right). \tag{3.8}$$

Where the parameter $\tau$ represents the length-scale parameter and needs to be learned from the data. For the general case of any kernel the parameter are described as $\boldsymbol{\theta}$. We can learn $\boldsymbol{\theta}$ by maximizing the marginal likelihood $p(\mathbf{y}|X, \boldsymbol{\theta})$ which is expressed as follows,

$$\log p(\mathbf{y}|X, \boldsymbol{\theta}) = -\frac{1}{2}\mathbf{y}^\top K_y^{-1}\mathbf{y} - \frac{1}{2}\log|K_y| - \frac{n}{2}\log 2\pi, \tag{3.9}$$

where $K_y = K + \sigma_n^2 I$.

In order to maximize the marginal likelihood, the partial derivative,

$$\begin{aligned} \frac{\partial}{\partial\theta_j}\log p(\mathbf{y}|X, \boldsymbol{\theta}) &= \frac{1}{2}\mathbf{y}^\top K_y^{-1}\frac{\partial K}{\partial\theta_j}K_y^{-1}\mathbf{y} - \frac{1}{2}\operatorname{tr}\left(K_y^{-1}\frac{\partial K_y}{\partial\theta_j}\right) \\ &= \frac{1}{2}\operatorname{tr}\left((\boldsymbol{\alpha}\boldsymbol{\alpha}^\top - K_y^{-1})\frac{\partial K_y}{\partial\theta_j}\right) \text{ where } \boldsymbol{\alpha} = K_y^{-1}\mathbf{y}, \end{aligned} \tag{3.10}$$

has to be solved.

Inverting the positive definite symmetric $n \times n$ matrix $K_y$ is computational expensive and requires the time of $\mathcal{O}(n^3)$.

The solution for the hyperparameters might result in a local maximum with each corresponding to a particular interpretation of the data (Rasmussen & Williams, 2005). This can cause different length-scale parameters for the same set of training data.

## 3.2 Random Forests

The RF is an instance of unsupervised learning that finds frequent use in the domain of ML. This thesis also makes use of RF, which are constructed by combining multiple decision trees.

### Decision Trees

A decision tree consists of a root node and connected nodes. The nodes at the end of the tree are called leaves. The leaves specify the output or the target for any given input that falls into that part of the input space. At each node $i$ a decision is made by comparing the feature $j$ to a threshold value $t_i$. Depending on the decision within the node, the feature input vector is further passed down, either to the right or to the left, to the next node or leave. (Murphy, 2022). A simple form of a decision tree and its output can be seen in Figure 3.2.

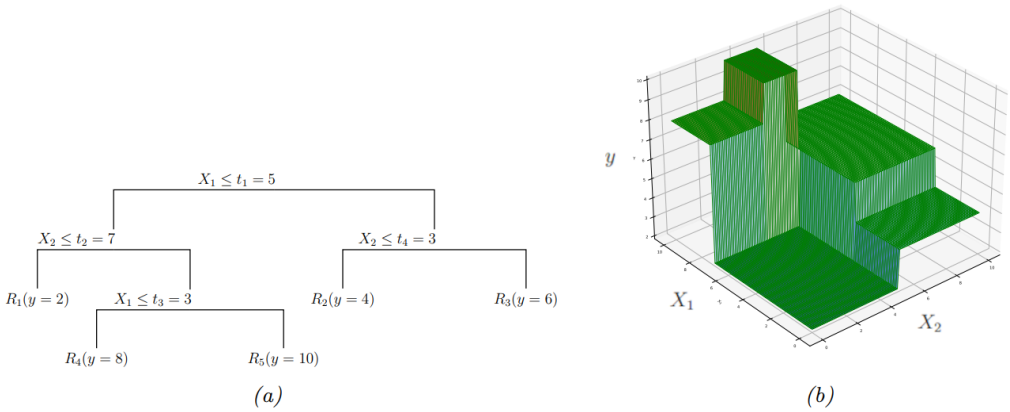


Figure 3.2: (a) Shows a decision tree with two decision features. (b) Shows the regression of the tree for a subset of testing variables from the two-dimensional input space, from Murphy, 2022.

The decision tree outputs a value corresponding to all the decisions made throughout the nodes. Those correspondences need to be learned during training to further use a decision tree for machine learning.

### Training

The decision tree does not have a typical continuous output function. Changing an input slightly can lead to a totally different prediction. This can be observed in Figure 3.2 (b). Furthermore, this implies, that the decision trees optimization equation is not differentiable. Important approaches to train a tree is therefore to grow a tree one node at a time. The threshold for the decision within a node needs to be evaluated. This is done by considering how the data reaching

the node $i$ can be further split with the least possible error in each child subtree. The data is partitioned at each node assuming the data contains just real valued scalars. Partitioning is done by comparing the data to a threshold $t$. The threshold is obtained by sorting the values within the input feature vector which is passed from upper nodes. If one value occurs multiple times just one is chosen. Multiple different thresholds are possible, but most of the trees are binary trees. Hence just one threshold is used in one node. In a binary decision tree, a left and a right split is created (Murphy, 2022).

A decision tree offers the advantage of allowing the use of both continuous and discrete values as a threshold, thus enabling the integration of regression and classification techniques. However, in the context of this thesis, only regression is of interest. The cost function,

$$c(\mathcal{D}_i) = \frac{1}{|\mathcal{D}|} \sum_{n \in \mathcal{D}_i} (y_n - \bar{y})^2, \tag{3.11}$$

where

- $i$: is the index of the node,
- $\mathcal{D}_i = \{(\boldsymbol{x}_n, y_n) \in N_i\}$: is the data set before the split at node $i$,
- $y_n$: is the target value,
- $\bar{y}$: the mean of the targets,

is used for a regression problem.

The process of computing a split for left and right, for each feature, for each threshold and for each node continues while building the tree from top to bottom. The best feature $j_i$ to split on and the best threshold value $t_i$ for that feature can be calculated by

$$(j_i, t_i) = \arg \min_{j \in \{1,\dots,D\}} \min_{t \in \mathcal{T}_j} \frac{|\mathcal{D}_i^L(j,t)|}{|\mathcal{D}_i|} c(\mathcal{D}_i^L(j,t)) + \frac{|\mathcal{D}_i^R(j,t)|}{|\mathcal{D}_i|} c(\mathcal{D}_i^R(j,t)), \tag{3.12}$$

where

- $\mathcal{D}_i^L(j,t) = \{\mathcal{D}_i : x_{n,j} \leq t\}$: is the left split of the data set at node i.
- $\mathcal{D}_i^R(j,t) = \{\mathcal{D}_i : x_{n,j} > t\}$: is the right split of the data set at node i.
- $t_i$: the threshold at node $i$.
- $j_i$: is the feature of the decision at node $i$.
- $i$: is the index of the node.

The data is then partitioned and the splitting algorithm is called recursively on each subset of the data (Murphy, 2022).

### Random Forests

RFs are an ensemble of multiple decision trees. One significant drawback of decision trees is that overfitting is a potential issue. Additionally, there is a possibility that a specific feature may be more influential than others.

It is for these reasons that the method of training multiple trees on subsets of the data was established. These subsets are randomly chosen. The rationale is that running the same learning algorithm on different subsets of the data will result in sufficiently diverse base models (Murphy, 2022).

The ensemble of multiple trees can be expressed as follows,

$$f(\boldsymbol{x};\boldsymbol{\theta}) = \sum_{m=1}^{M} \beta_m F_m(\boldsymbol{x};\boldsymbol{\theta}), \tag{3.13}$$

where:

- $F_m$: is the $m$-th tree
- $\beta_m$ is the weight corresponding to each tree.

Usually, the weight is set to be $\beta_m = 1/M$, whereas $M$ is the total number of trees.

### Feature Importance

Feature importance is a method used to analyse which dimensions of the input feature vector are most influential on a model's decisions. It shows how much a feature helps to reduce prediction error. It is calculated by adding up the decrease in Mean Squared Error from splits involving the feature across all trees. High importance scores indicate features that significantly reduce prediction error, while low scores suggest features with minimal impact. (Ronaghan, 2019).

# 4 Regression of Time Temperature Transformation

The task is to predict the TTT for bainitic steel. The accuracy of state-of-the-art systems to estimate the TTT is limited. Traditional physics-based models assume linear correlations between variables. In this thesis, the focus lies on machine learning approaches to estimate the TTT for any given steel alloy in a purely data driven manner. At first the idea was to use Neural Networks (NNs) and GPRs to solve the regression for mapping the input, which consists of the weight percentage $w_{per}$ and the iso-thermal holding temperature $T_H$ at which the measurement was taken.

The NNs did not create sufficient predictions because of various reasons. One of them is that the data gathered from scientific papers had less samples than the data from experiments. This imbalance causes the NN to perform better on the overrepresented experimental data while underperforming on the underrepresented scientific paper data. Additionally, experiments lasting up to 60,000 seconds widen the range of available samples and further increase the amount of data within a measurement. This further implies that the NN and the GPR needs more time to train, because the computational complexity is increased by $\mathcal{O}(n^3)$. Unfortunately, the performance of using NN to estimate the phasefraction curve $f_B$ did not create sufficient prediction results, as shown in Figure 4.1.

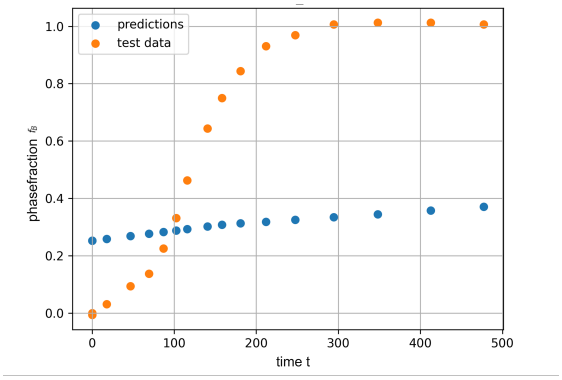


Figure 4.1: Predictions of the phase fraction curve using a NN for regression. An example for insufficient prediction results.

Each sample from one sigmoidal-shaped phase fraction has the same input features, i.e., the material composition and the iso-thermal holding temperature stay constant throughout one measurement. This property was used to reduce the complexity of the problem introduced in the following section.

## 4.1 The t90% Problem

Reducing the number of samples per measurement was key in terms of simplifying the problem. For this, a new metric was introduced. The idea is, that one dilatometry experiment is described by one value. The new target value was chosen to be the time at which the phase fraction reaches 90% of its maximum value. Interpolation between discrete measurements was used to find the exact value, as it is unlikely that there is a measured sample for the exact value of 90%. This introduces a small error, which can be neglected.

In Figure 4.2 the concept of using one value to describe one measurement is shown. It shows one material which was measured with seven different iso-thermal holding temperatures. The red dots indicate the t90% value and the red line is the interpolation connecting the dots. The shape of the red line is similar to the c-shape from the TTT diagram, which is explained in Section 2.1.

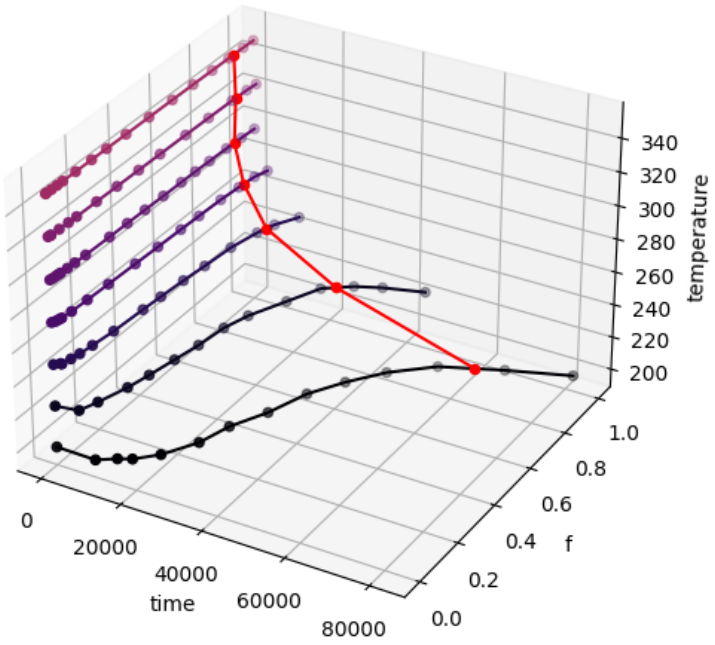


Figure 4.2: Multiple measurements from the dilatometry experiments from seven different iso-thermal holding temperatures. The red dots indicate the t90% value for each measurement.

Through this the number of samples used for describing the material is reduced from 91 measured samples to seven samples (i.e. one for each $T_h$), without losing information. Figure 4.3 gives a better insight on how the data is simplified. Figure (a) is the original data which is the phase fraction measurement curve depending on the time $f_B(t)$ and Figure (b) shows how the data looks after determining the t90% value which is depending on the temperature. This shows clearly how the t90% measurement forms part of a c-shape over the multiple measurements by simply interpolating between the new gathered t90% values.

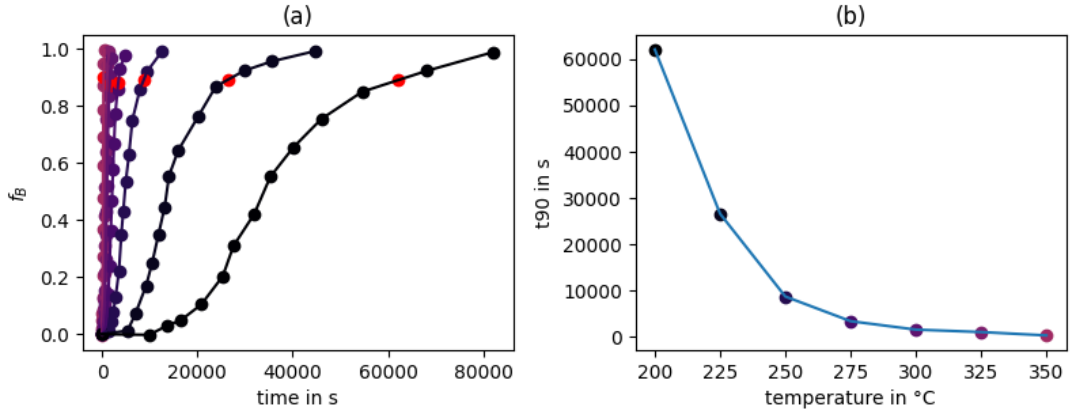


Figure 4.3: Multiple measurements from the dilatometry experiments from seven different iso-thermal holding temperatures (encoded by color from black to light purple) within the same steel alloy. (a) The samples are dependent of the time and the red dots indicate the time at which 90% of the final phase fraction was reached. (b) Part of the c-shape formed by the t90% values for different temperatures.

The introduction of this simplification reduces the amount of data and enables faster training. Especially for the GPR this is an advantage, because the kernel matrix is reduced in its size and there are less parameters to be optimized.

### 4.1.1 Data Preparation

Filtering the data before training the model was done to avoid learning wrong relationships. This requires knowledge about the physics and the behaviour of the dilatometry experiment. The phase fraction, for example, always starts at the value of $f_B(0) = 0$ and the shape of the function measured is similar to the sigmoid function. Any phase fraction measurement which did not reach a maximum of $f_B(t_\infty) = 0.15$ was neglected. A further problem of the given data was that for some samples it was not possible to say if the measurement was stopped before the maximum dilatation. Therefore the last sample within a measurement was considered to be the one at full expansion.

Each material contains multiple dilatometry experiments, which result in one t90% value. The t90% which is derived from the phase fraction $f_B(t)$ depends

on the weight percentage of each element within the steel alloy $w_{per}$ and the temperature at iso-thermal holding $T_H$. The number of materials is $k$ and the number of dilatometry experiments is $n$. This information is put into the following shape,

$$X_{\text{input}} = \begin{bmatrix} \mathbf{w}_{\text{per}_0} & T_{0,0} \\ \mathbf{w}_{\text{per}_0} & T_{0,1} \\ \vdots & \vdots \\ \mathbf{w}_{\text{per}_0} & T_{0,n} \\ \mathbf{w}_{\text{per}_1} & T_{1,0} \\ \vdots & \vdots \\ \mathbf{w}_{\text{per}_k} & T_{k,n} \end{bmatrix}, \quad y_{\text{target}} = \begin{bmatrix} t_{90\%0,0} \\ t_{90\%0,1} \\ \vdots \\ t_{90\%0,n} \\ t_{90\%1,0} \\ \vdots \\ t_{90\%k,n} \end{bmatrix}. \tag{4.1}$$

### 4.1.2 Results for t90% Values

Even though the problem was easier to solve for the ML models the test performance never reached satisfactory results and further discussion about how the models could be improved was conducted. The simplified problem is still a hard problem to solve by the ML models and the training with a limited number of training data does not give sufficient results for the predictions. An alloy of steel with a small change in weight percentage for a specific element gives a large difference in the output. This is challenging for the model and did not get resolved by simplifying the problem. Furthermore, the target to be estimated, hence the duration of the experiment, spans a wide range, from seconds to several hours.

Figure 4.4 shows the difficulty of the GPR learning the huge value span in terms of the target. The trained ML model reacts heavily to small changes, therefore the estimate of the first sample at an iso-thermal holding temperature of 300 °C is far from the real value. Negative duration to reach $t90\%$ is not even possible, but the model estimated it as such.

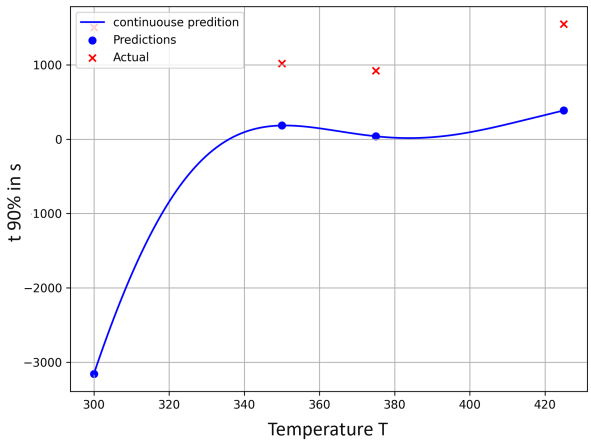


Figure 4.4: Using a GPR to estimate the t90% targets for material 13. The estimated negative t90% value for T = 300°C is a result of high sensitivity of the model due to the high range of possible target values.

In Figure 4.5 another effect of huge numbers and similar input features can be observed. The estimated curve of the GPR for material number 0 oscillates around the real-valued data. This effect originates from the high sensitivity of the model, causing oscillations. High sensitivity means that a small change in the input, for example the iso-thermal holding temperature, can cause a big change at the output. This can be observed in Figure 4.3, where a change of 25°C causes the dilatometry experiment to take 8.3 hours longer.

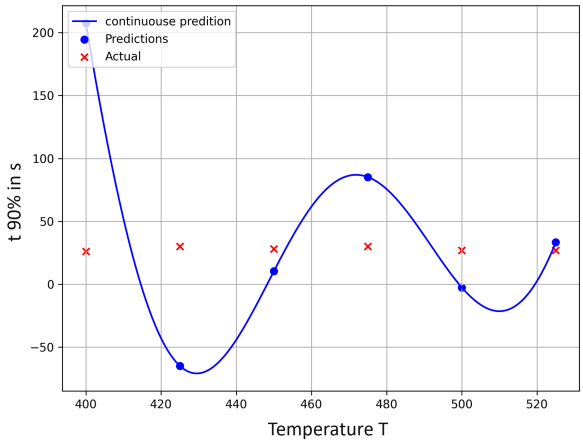


Figure 4.5: Using a GPR to estimate the t90% targets for material 0. The predictions oscillate due to the high sensitivity of the model.

## 4.2 Improving the GPR

The GPR prediction results for t90% predictions were better but still not sufficient. This is fixed by introducing a relative error to improve the model. Adding

additional information with more input features also leads to a better predicting GPR model.

### 4.2.1 Log Transform of Target Values

Dealing with a wide range of target values presents a challenge in ML training. To address this, a logarithmic transformation is used. The logarithmic function compresses larger values more than smaller ones, reducing the span between target values. After the logarithmic transform the target values represent a more uniform distribution. Additionally, the logarithmic transformation helps to stabilize the variance which makes the target values more homoscedastic. The measurement error from the dilatometry experiment is heteroscedastic and therefore increases as the time of bainitic transformation increases, i.e.,

$$\epsilon_i \sim \mathcal{N}(0, \sigma_n^2 \, y_{target_i}). \tag{4.2}$$

After applying the logarithmic transform to the the representation changes as follows:

$$\log(y_{target_i}) = \log(f(X_{input_i})) + \tilde{\epsilon}_i. \tag{4.3}$$

To further encounter the problem of heteroscedastic noise, a GPR can use the inverse information of the target value $y_{target}$. In GPR with inverse weights, we modify the standard approach by incorporating weights that are inversely related to the uncertainty or importance of each data point, effectively adjusting the influence of each observation based on the value of the target and the measurement error.

Figure 4.6 shows the predictions of a GPR without the logarithmic transformation on material 42. The blue line is the prediction between the real data points, which are indicated by the red x's. The advantage of the GPR is, that it shows how certain it is for a specific estimate. This is expressed as the covariance value for each prediction point. Further, this is shown in the plot as the light blue area, which indicates that the value lies within this blue area with a certainty of 95%.

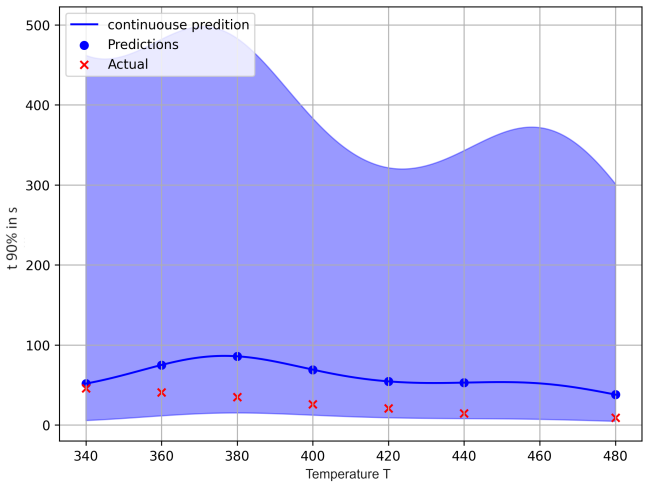


Figure 4.6: Applying the GPR to the input set of material 42. The light blue area shows the 95% confidence interval. The GPR's predictions are subject to high uncertainty.

In Figure 4.7 the GPR with logarithmic transformation of the targets is used to make predictions on the same materials as in Figure 4.6.

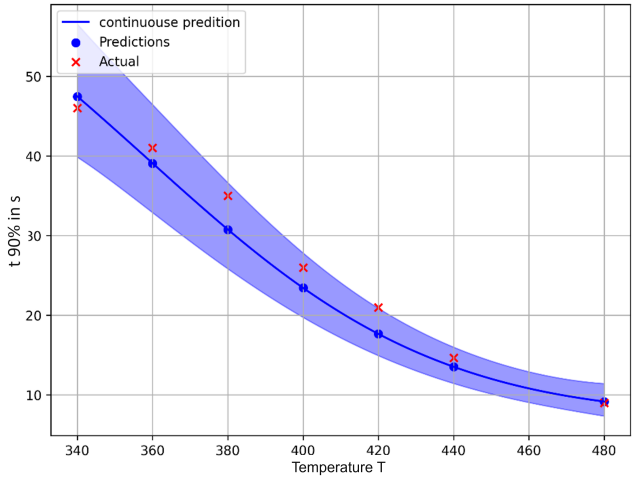


Figure 4.7: Applying the GPR with log-transformed targets and inverse weights to the input set of material 42. The light blue area shows the 95% confidence interval. Due to the logarithmic transformation of the target values, the uncertainty of the GPR's estimations is larger for larger targets and vice versa.

Introducing the logarithmic transformation as well as adding inverse weights during training is an improvement to the model's predictions.

### 4.2.2 Supercooling

Supercooling is a phenomenon observed when a substance is cooled below its typical freezing point without immediately solidifying. This occurrence

is common with pure substances such as water or ice. In the case of ice, supercooling allows it to persist in a liquid state below its standard freezing point of 0 °C until a trigger prompts crystallization.

Each feature dimension provides valuable information for the model, which utilises this information for making predictions. By adding a new descriptor to the input features more knowledge is given to the ML model. The new descriptor depends on the bainite start temperature $Bs$ and holds information about the highest possible temperature at which bainite can form.

The elements within the alloy influence the value for the $Bs$ descriptor, calculated as follows, i.e.,

$$Bs = 746 - 162 \cdot w_C - 16 \cdot w_{Si} - 73 \cdot w_{Mn} - 53 \cdot w_{Cr} - 44 \cdot w_{Mo} - 29 \cdot w_{Ni}, \quad (4.4)$$

where the constant coefficients have been determined by empirical analysis.

The $Bs$ descriptor is influenced by both the compound and the temperature of each sample. It gauges the distance from the current temperature to bainite start temperature. The $Bs$ descriptor for each iso-thermal holding temperature is calculated as,

$$Bs(T) = Bs - T. \quad (4.5)$$

Adding the additional $Bs$ descriptor to the input vector from Equation 4.5 results in the following input and output data,

$$X_{\text{input}} = \begin{bmatrix} \mathbf{w}_{\text{per}_0} & T_{0,0} & (Bs_0 - T_{0,0}) \\ \mathbf{w}_{\text{per}_0} & T_{0,1} & (Bs_0 - T_{0,1}) \\ \vdots & \vdots & \vdots \\ \mathbf{w}_{\text{per}_0} & T_{0,n} & (Bs_0 - T_{0,n}) \\ \mathbf{w}_{\text{per}_1} & T_{1,0} & (Bs_1 - T_{1,0}) \\ \vdots & \vdots & \vdots \\ \mathbf{w}_{\text{per}_k} & T_{k,n} & (Bs_k - T_{k,n}) \end{bmatrix}, \quad y_{\text{target}} = \begin{bmatrix} t_{90\%0,0} \\ t_{90\%0,1} \\ \vdots \\ t_{90\%0,n} \\ t_{90\%1,0} \\ \vdots \\ t_{90\%k,n} \end{bmatrix}. \quad (4.6)$$

# 5 Results and Discussion

To determine how the model performs on unseen data, a strategy involves using most of the samples from the data set for training and the rest for testing. Our data set is relatively small in comparison with the number of input features associated with the problem. Consequently, a distinct evaluation methodology is required. For this use case leave-one-out training is used. This allows a good analysis on the performance of the ML models even though it requires longer training.

The materials are indexed from 0 to the number different steel alloys provided, which in this case is 55. To enhance readability, the alloyed materials are referenced by their indexed number from the data set, rather than by their name.

## 5.1 Results

The ML models used for the results are the RF and the GPR with inverse weights. The target was transformed using log transformation. For comparative purposes and discussions, each ML model was trained with either the full input features available or a reduced set of features. Two different input feature vectors were used for training and testing: The full feature set includes: Fe, C, Si, Mn, Cr, V, Co, Al, N, B, P, Ti, S, W, Cu, Mo, Ni, Nb, the iso-thermal holding temperature $T_H$ and the descriptor $Bs$. The reduced feature set includes: C, Si, Mn, Cr, Mo, Ni, the iso-thermal holding temperature $T_H$ and the descriptor $Bs$.

The Mean Absolute Percentage Error (MAPE),

$$\text{MAPE} = \frac{1}{n}\sum_{i=1}^{n}\left|\frac{t_{90i} - \hat{t}_{90i}}{t_{90i}}\right| \cdot 100, \tag{5.1}$$

where:

- $n$ is the number of samples,
- $t_{90i}$ is the true t90% value of the $i$-th sample,
- $\hat{t}_{90i}$ is the predicted t90% value of the $i$-th sample,

is used to determine the prediction accuracy of the ML models.

It is preferred to use a MAPE over an absolute error for determining prediction accuracy of the ML models. For example, the prediction error of 100

seconds is tolerable for an experiment lasting 60000 seconds, but not if it takes only 200 seconds. This can be expressed by using the MAPE. The MAPE error of the RF predictions with the reduced input features are presented in Figure 5.1 and the results for the GPR with the reduced feature set is shown in Figure 5.2.

The MAPE is most of the time between 50% and 100%. For a few predictions the MAPE could be below 50% for both the GPR and the RF with either the full or the reduced feature input vector. The RF model, which included information about all elements, predicted 10 materials with an error larger than 100%. The RF model, which included the reduced feature set, predicted 13 materials with an error larger than 100%. This states, that the prediction accuracy of the RF is increased by using the full feature set.

Not a single ML model used could predict material 2, 15. 41 and 44 with decent accuracy, hence the MAPE is larger or around 100%.

The RF with the full feature set predicted material 6 with an MAPE below 10%. This accuracy could be achieved by the GPR with the reduced input features for material 21.

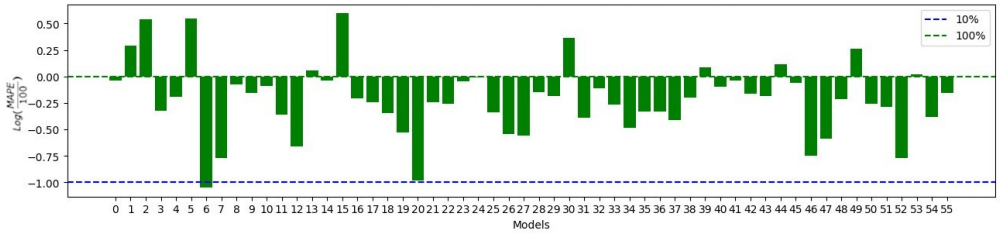


Figure 5.1: Logarithm of the MAPE for predictions from the RF with the full input features. The green dashed line shows an error of 100% and the blue dashed line shows an error of 10%.

The GPR with the full feature set has worse prediction performance compared to the GPR with the reduced feature set. A direct comparison of the RF with the GPR reveals that the GPR with reduced feature set has a greater number of predictions below a prediction error of 100%.

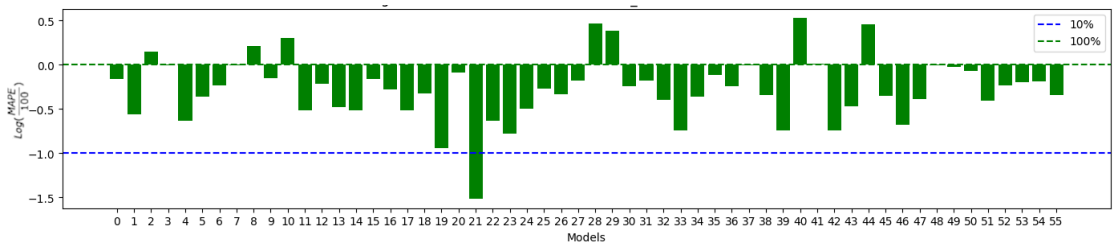


Figure 5.2: Logarithm of the MAPE for predictions from the GPR with the reduced input feature for each material. The green dashed line shows an error of 100% and the blue dashed line shows an error of 10%.

Compared to the RF with the full feature set, the GPR with the reduced feature set has poor performance on the left-out materials 3, 7, 20, 28, 29, 37 and 54. The GPR performs better on materials 1, 5, 16 and 30 than the RF models.

High prediction errors are caused by the fact that there are no similar materials in the data set with similar behaviour during the dilatometry experiment.

One of the key advantages of the GPR is its predicted uncertainty. The uncertainty provides insight into the degree of certainty associated with a given prediction. This measure is derived from the kernel matrix and is expressed in the form of the standard deviation. It can be employed to calculate a confidence interval. The standard deviation for each leave-one-out measurement of GPR using the reduced feature set is shown in Figure 5.3.

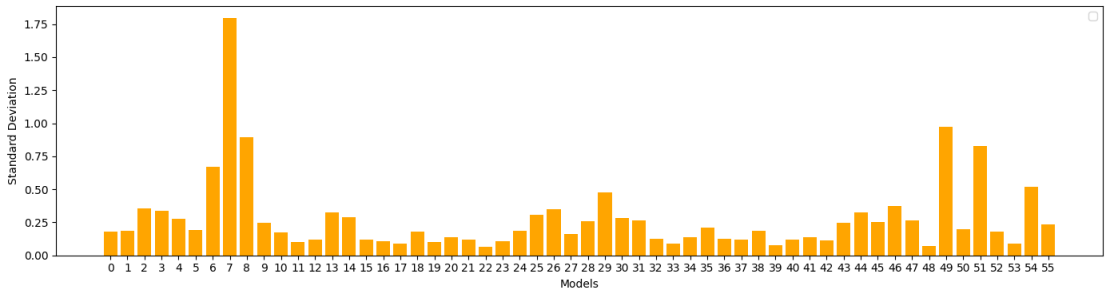


Figure 5.3: Standard deviation for predictions from GPR for each model.

The plot indicates how certain the GPR is about its predictions. The GPR is uncertain especially for the materials 6, 7, 8 and some of the unconventional materials 49, 51 and 54. Combining the information of the MAPE error and the standard deviation the performance of the GPR is very clear. Model predictions with a low prediction error and a high standard deviation are not trustable. For example, the model for estimating material 6 shows a high standard deviation, but a low MAPE.

## 5.2 Discussion

Comparing GPR models can be done by using the covariance function for each dimension, which is further expressed by the length-scale parameters. The length-scale gives information about the degree of correlation within one input feature. For instance, the length-scale parameter for the iso-thermal holding temperature $T_H$ is very small throughout all the trained models. This means that the t90% target value is strongly depended on that feature. The higher the length-scales of a input feature the lower the influence to the output. For evaluating the models, the length-scale matrix is plotted. This in addition to the leave-one-out method gives insights of how different the models are to each other. Contrasting materials in the training set can change the length-scales to have more weight on a specific element or a feature.

The length-scale parameters shown in Figure 5.4 give an insight of how important each individual input feature is for the later prediction of the model. These values are trained during the leave-one-out training. The length-scale parameters for each leave-one-out training iteration are presented in a separate row. The row index is identical to the index of the material that was excluded during the leave-one-out training. Running a model multiple times should result in the same or similar solutions and similar predictions. This further leads to identical length-scale parameters. However, in the column of iron the lighter blue indicates that iron was learned to be more important for that specific training set. ML models can either focus on the absence of iron or on the additional percentage that other elements have instead of iron. Chrome (CR), Vanadium (V), Phosphorus (P) and Copper (C) have a length-scale parameter above one, which indicates that those elements do not have a lot of effect according to the model. The effect of different length-scale parameters of a feature even though only one material has been exchanged between one row is further explained in Section 5.2.1.

The number of input features was decreased to the reduced set based on the elements that are known to have major effect on the output, hence the behaviour of the steel. The reduced input results in a faster converging GPR, or in faster training, in general, because the number of parameters to optimize is decreased. This setting makes the GPR more robust because it is not tempted to weight unimportant elements more than others. Training both the one with all the features (i.e. full feature set) and the one with selected features chosen (i.e. reduced feature set) is an effective method to gain a deeper understanding of the training process. Figure 5.5 illustrates the length-scale for the GPR for the reduced feature set. It can be observed that the elements of interest exhibit a greater degree of similarity in length-scale parameters throughout the training process. However, it is important to note that the leave-one-out method has the potential to enhance the comparability of length-scale parameters. The property of exchanging just one material from the test set to the training set should

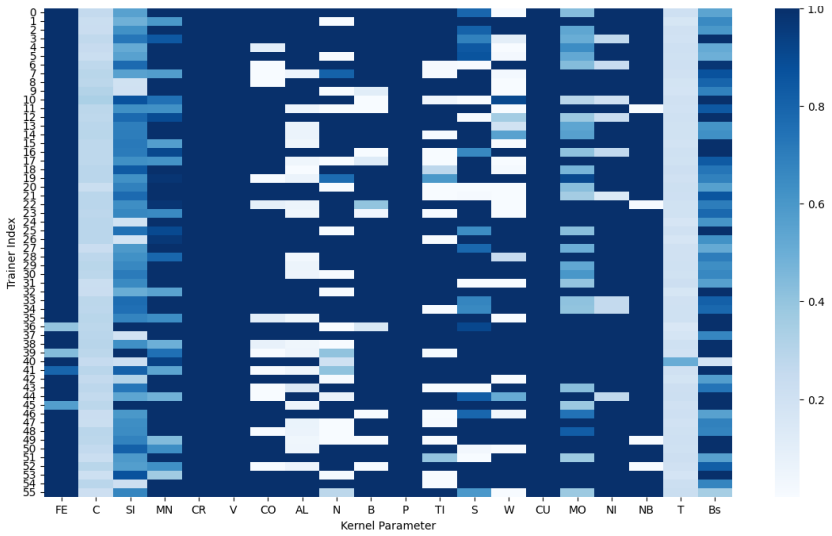


Figure 5.4: Lenght-scale parameters for each input feature and trained model. If the length-scale is larger than one it is set to one.

not significantly influence the length-scale parameters. It can be observed that chrome is still not a particularly important feature for the GPR model within the reduced feature set. This can be observed in the length-scale matrix of Figure 5.5.

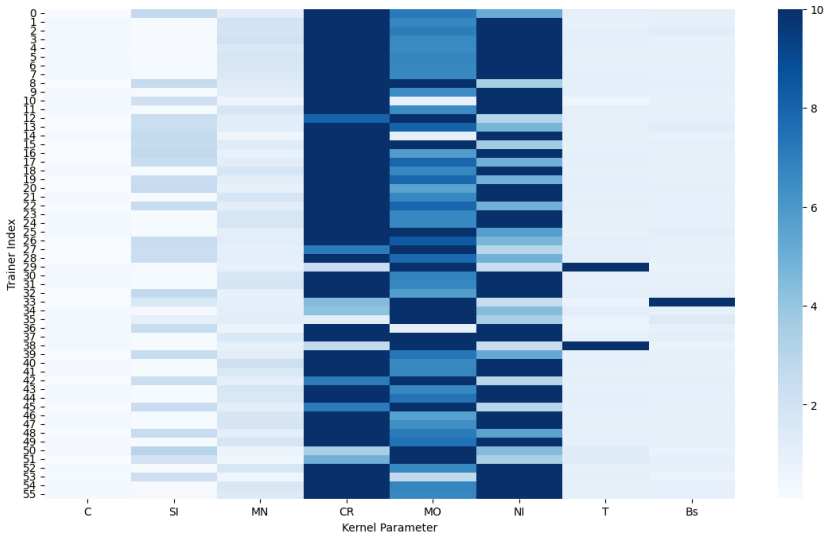


Figure 5.5: Lenght-scale parameters for the GPR with a reduced feature set. If the length-scale is larger than one it is set to one.

The RF has a similar approach for assessing the importance of the model parameters. In a RF, input features are used for making decisions within all the trees. A feature used in more nodes is more important. This creates a

feature importance vector for every RF model. Figure 5.6 illustrates the feature importance matrix for the entire leave-one-out test set. It demonstrates that the features within the RF are almost equally important across the columns. This indicates that the RF identifies similar feature importance across the 56 distinct trained RF models from the leave-one-out method.

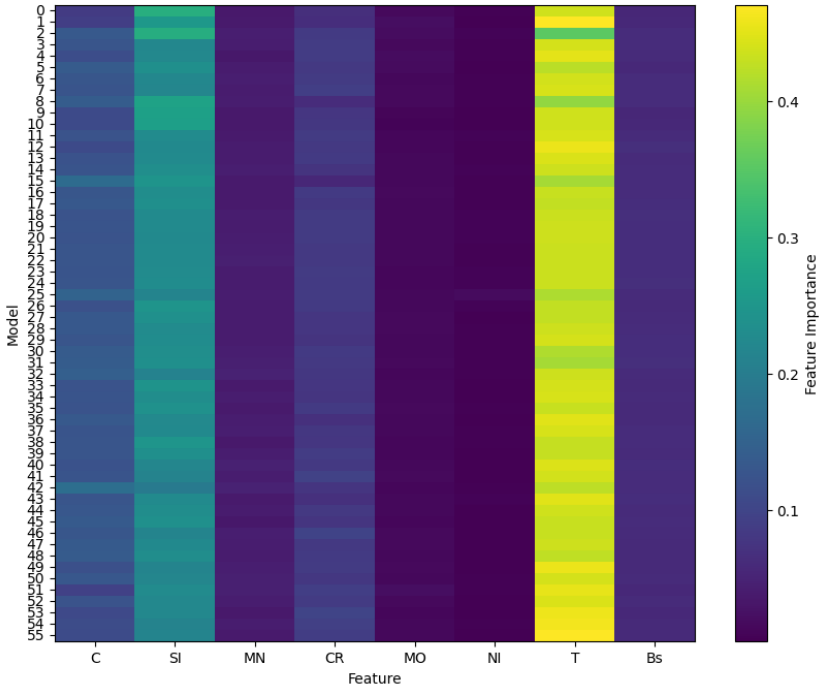


Figure 5.6: Feature importance matrix from RF models with reduced features over all materials. If the length-scale is larger than one it is set to one.

The reason for following predictions is often a lack of coverage in certain areas of the data. This section covers some of the material predictions of higher errors and less accuracy. The reason why a model cannot find good predictions for the reduced feature set is also further discussed.

### 5.2.1 Convergence Behaviour of the GPR

The observation of identical length-scale parameters across all training scenarios is indicative of the GPR converging to a consistent solution. Conversely, the absence of such parameters suggests that the GPR may be oscillating between multiple local minima or failing to converge altogether. This phenomenon may be attributed to the pivotal role of the kernel parameters in the model's initialization. A leave-one-out training approach was employed, wherein the same material was used for training on each iteration, to assess the impact of random hyperparameter initialization on the convergence behaviour of the GPR. The model parameters should be identical training on the same train and test

split multiple times. This is evidenced by the observation that the length-scale parameters are the same for each training set. Material 0 was the material being left-out, and training was done on all the other materials. Figure 5.7 shows how multiple training runs on one case leads to different length-scale parameters. With this method, it can be argued that the GPR does not find the same solution for each training. One simple method to circumvent this issue is to set a lower bound on the length-scale parameters in each dimension, which does not allow the GPR to learn the length-scale parameter below this bound. A higher lower bound reduces the probability of the GPR focusing on a single element. This is a means of avoiding overfitting. Figure 5.8 illustrates how modifying the lower bound leads to a more uniform distribution of learning. Various models may employ the same solution for the length-scales, yet due to the limitations of the length-scale, the resulting predictions may not be sufficient and the model may be underfitted. Therefore, setting the lower bound is of importance and is partially the determining factor for the selection of optimal hyperparameters. A lower bound of $10^{-7}$ allows for more specific training, although the length-scale parameter varies considerably.

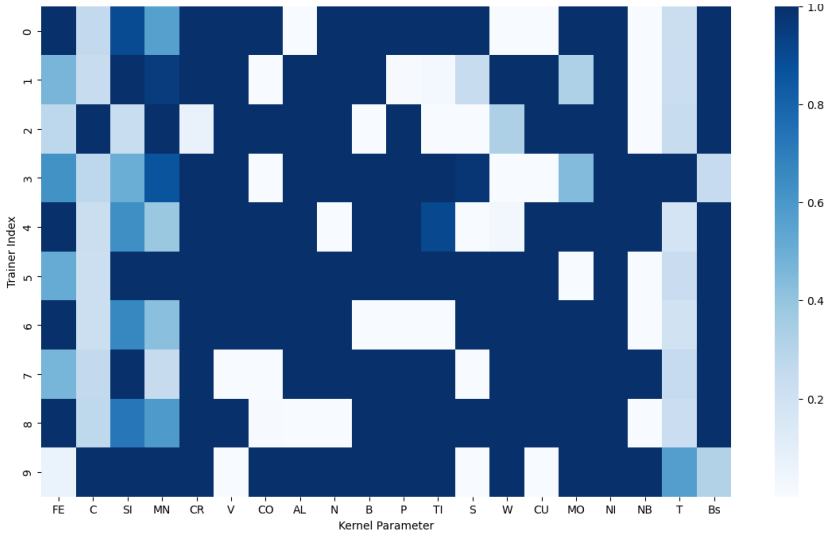


Figure 5.7: Setting a lower bound of $10^{-7}$ for to the length-scale parameters allows more specific training, however the length-scale parameter vary a lot. 10 training runs (rows) on the same data set.

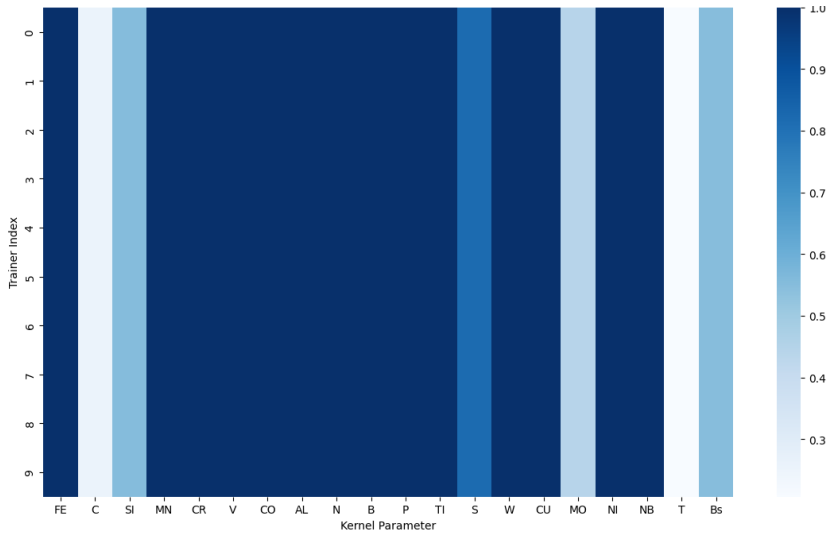


Figure 5.8: Limiting the lower bound of the length-scale decreases overfitting. The lowerbound was set to $10^{-2}$. 10 training runs (rows) on the same data set.

### 5.2.2 Low Temperatures

The measurements preferred in industry are typically conducted at a limited number of temperatures, whereas fundamental researchers gather data over a wider range of temperatures. Therefore, the scarcity of data in specific areas of the data set results in suboptimal predictions. This is due to the lack of information in the specific area of the feature space. Therefore, the mapping from the input to the output is not well known to the model. The prediction error for materials with measurements below and above a certain temperature can be high. The distribution of the different iso-thermal holding temperatures used for the measurement can be seen in Figure 5.9. Most temperatures are measured between 250°C and 500°C. As a result, the model lacks substantial data for most measurements and materials outside this temperature range. From a knowledge perspective, the model can observe a greater number of samples points within this temperature range. The error at the lower temperatures or the higher temperatures is greater than in those areas where there is more knowledge about certain temperatures. Depending on the source of the measurements the availability of additional data samples within the temperature range may vary.

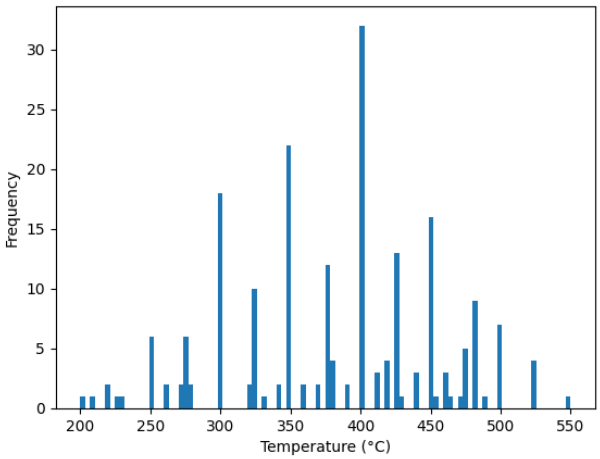


Figure 5.9: Distribution of iso-thermal holding temperatures of all experiments.

An illustrative example of this phenomenon is provided by material number 2. Figure 5.10 depicts material 2. It can be observed that as the temperature decreases, the accuracy of the model predictions get worse. Furthermore, the confidence of the GP, either with all the elements or with the most important elements, increases as the temperature decreases. It is important to note that a measurement that takes up to 6000 seconds is not of interest to the industry, as there is no practical use case for such a slow transformation.

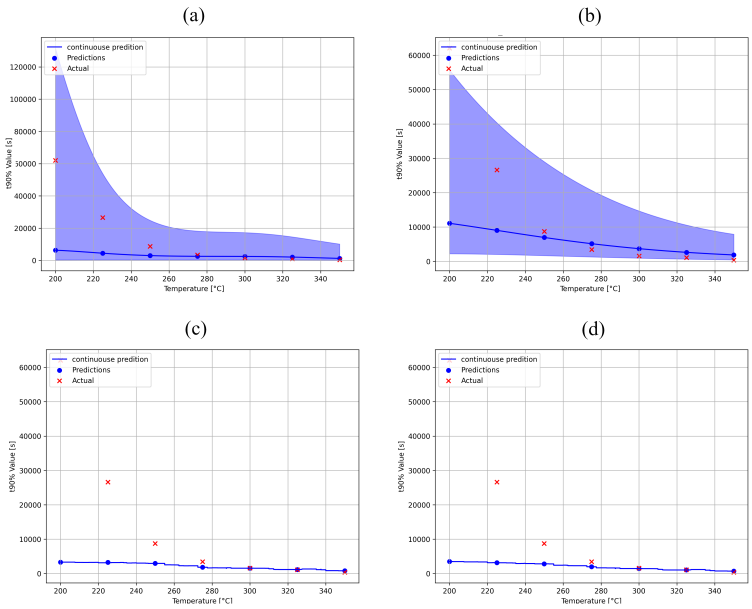


Figure 5.10: Example for uncertain predictions below 250°C of material 2. (a) GPR using full feature set, (b) GPR using reduced feature set, (c) RF using full feature set and (d) RF using reduced feature set.

### 5.2.3 Boron

In the absence of information regarding the influence of a specific element on the behaviour of the compound, the predictions of the ML model are likely to be inaccurate. To illustrate, if there is no instance of a material containing boron in the training data, the model will be unable to ascertain the impact of boron on the output. The t90% value may be reached in a longer or shorter time, or that the additional value of boron will have no effect. Furthermore, it is possible that the percentage of boron is missing somewhere else, for example, there is less carbon or less chrome in the compound, which could also lead to a different behaviour. Therefore, this is a very challenging issue for any type of non-parametric ML model. The optimal solution to this problem is to incorporate a greater variety of materials with a wider range of compounds to encompass a more comprehensive spectrum of behaviours.

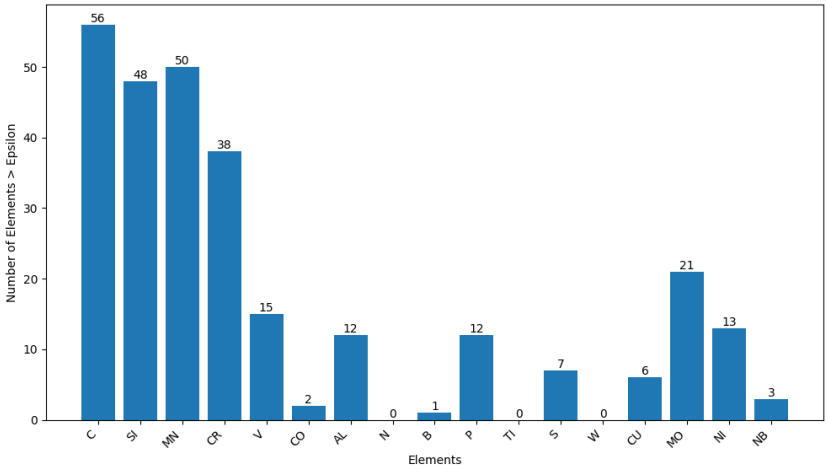


Figure 5.11: Number of occurrences for each element within the given data set.

Figure 5.11 demonstrates that material 15 is the sole element containing boron. None of the models tested were able to provide accurate predictions for the leave-one-out test case, with material 15 being excluded during training. Furthermore, the GPR demonstrates its uncertainty by increasing the confidence interval. Figure 5.12 illustrates the prediction from the GPR and RF.

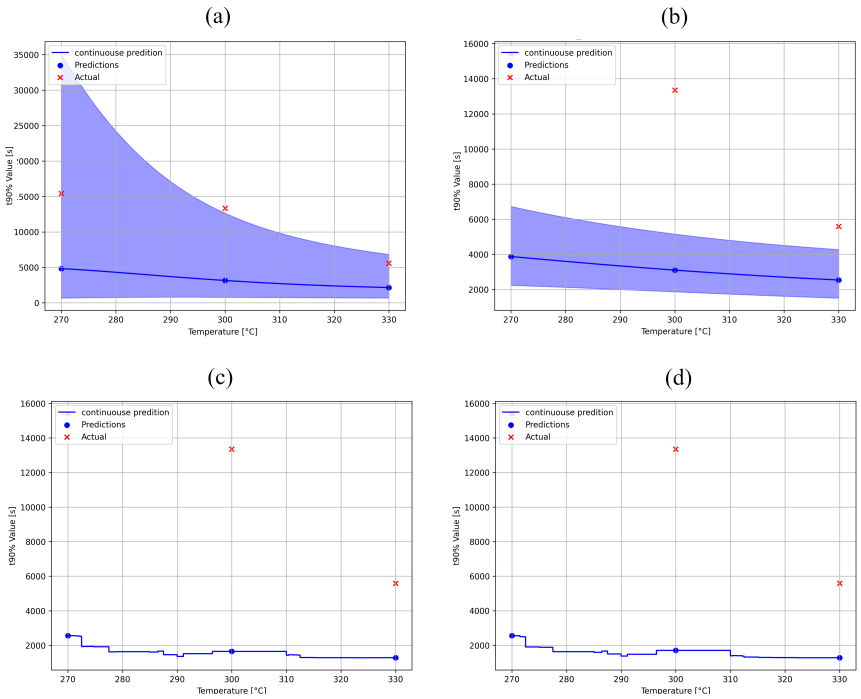


Figure 5.12: Prediction for material 15 which is the only material containing boron. (a) GPR using full feature set, (b) GPR using reduced feature set, (c) RF using full feature set and (d) RF using reduced feature set.

The predictions are unfavourable and the uncertainty is considerable. Despite the real values are not within the confidence interval predicted by the GPR, the change in behaviour due to the different compound is significantly greater than that predicted by the GPR. Additionally, niobium is present in the alloy. Niobium, like silicon, is not a highly represented element in the data set, and may have additional effects. Furthermore, there is limited knowledge available about the behaviour of niobium in this context.

### 5.2.4 Material 14

This material contains aluminium. Upon initial observation, it appears to be similar to other alloys. There are other materials that contain aluminium as well. Figure 5.11 illustrates that there are 11 other alloyed steels containing aluminium. Figure 5.13 depicts the quantity of aluminium present in each of the 12 materials containing aluminium.

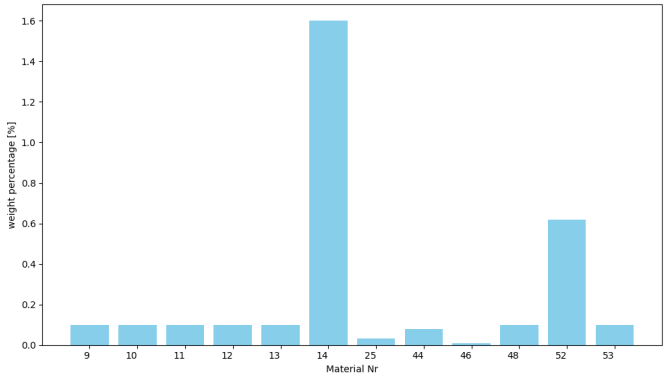


Figure 5.13: Amount of aluminium in weight percent for the 12 materials.

The bar chart indicates that material 14, which exhibited poor estimation, contains the greatest quantity of aluminium. The remaining materials, with the exception of material 52, exhibited a percentage of aluminium below 0.2%. According to the material scientist, the limited quantity of aluminium does not alter the measurement behaviour of material number 14. The GPR estimation error is larger than 100% if the lower bound is not limited during training. A GPR with the reduced feature set and a lower bound limit of $10^{-6}$ achieved predictions with a MAPE lower than 100%.

### 5.2.5 Silicium

The alloyed steels 3, 4, 5, 6, and 7 are composed of the same elements. The RFs predictions for these materials are generally accurate, except for model number 5. Results are shown in Figure 5.14. The RF model's prediction error for Material 5 is larger than 300%, whereas those for Materials 3, and 4 are lower than 100%, those for Materials 7 lower than 50% and those for Material 6 are even lower than 10%. A more detailed examination of the compounds listed in Table 5.1 reveals that the amount of silicon in material 5 differs significantly from other alloys. Material 5 has the lowest amount of silicon, which may explain why it behaves differently than the other materials. This discrepancy may be the reason why the RF models predict values that are significantly different from the actual measurements.

| Material Nr. | 4 | 5 | 6 | 7 |
|---|---|---|---|---|
| Fe [%] | 96.572 | 97.613 | 94.447 | 93.53 |
| C [%] | 0.448 | 0.452 | 0.443 | 0.43 |
| Si [%] | 1.2 | **0.225** | 3.34 | 4.28 |
| Mn [%] | 1.78 | 1.71 | 1.77 | 1.76 |

Table 5.1: Comparing different materials with similar composition

The GPR with the full feature set does not cover the real target values for material 5 within the confidence interval. The GPR with the reduced feature set has the best predictions since the uncertainty covers the real world data and the MAPE is the lowest. The MAPE and uncertainty interval of the GPRs predictions with the reduced feature set is large for material 7, which has the largest amount of silicium in its compound.

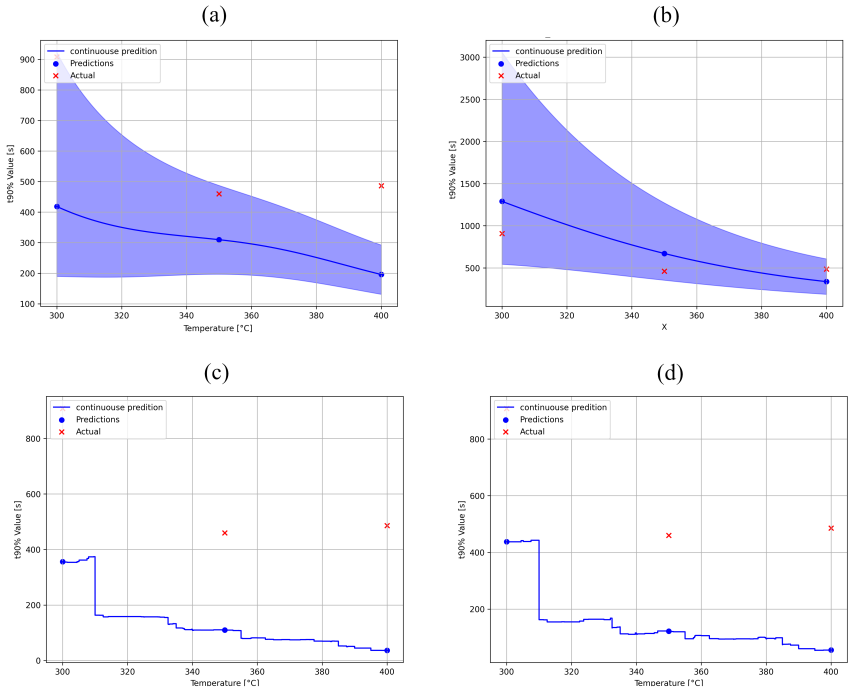


Figure 5.14: Prediction on all four models on material 5. (a) GPR using full feature set, (b) GPR using reduced feature set, (c) RF using full feature set and (d) RF using reduced feature set.

### 5.2.6 Effect of Similar Input Features

It can be observed that materials 16 and 26 share similar feature elements, resulting in a comparable compound. The model is aware of at least one other material within the same range of the feature space. This could potentially lead to more accurate predictions for these materials. In the leave-one-out method, the model either knows material 16 or material 26 during training. By comparing the t90% values for both materials at the same temperature, it is possible to assess the similarity of the measurements. Material 16 has reached 90% of its elongation within the experiment after 110 seconds at a iso-thermal holding temperature of 400°C, which is comparable to material 26.

Material 26 has a greater number of measurements at a temperature below 400°C. It is of interest to predict material 26 with the knowledge of material

16 during training. The GPR and RF yield more accurate predictions of the temperature at approximately 400°C. In particular, the GPR results in greater uncertainty in the feature input space for unknown points.

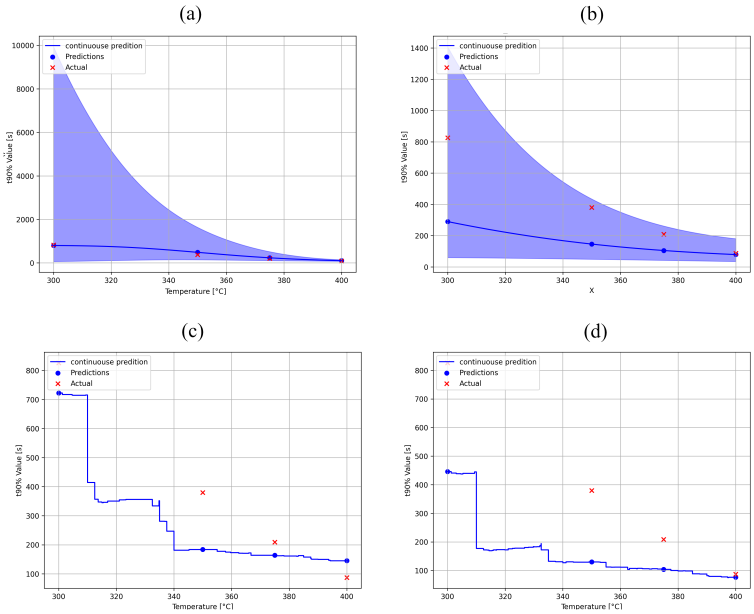


Figure 5.15: Predictions for measurements of material 26. (a) GPR using full feature set, (b) GPR using reduced feature set, (c) RF using full feature set and (d) RF using reduced feature set.

Figure 5.15 shows the result for material 26. The estimation of all the models at the known temperature with knowledge about another material with the same composition is highly precise. It is within degrees Celsius, which is not achievable for many other measurements. For the other sample points at 300°C, 350°C and 375°C, both GPRs exhibit increased uncertainty. Both GPRs significantly increase the uncertainty of the predictions, despite the mean of their predictions being satisfactory. The GPR with all the elements demonstrated superior performance to the one with the reduced feature set. The RF demonstrated robust predictive capabilities, thereby confirming the a priori expectation that the GPR with greater knowledge about a greater number of elements will yield more accurate predictions than the GPR with a smaller input vector.

## 5.3 Other Microstructures

### 5.3.1 Ferrite

The whole thesis is experimentally based on measurements of bainitic steel. However, the results for ferrite show that ML models have the potential to be applied to other microstructures. Academic measurements from Huang et al., 2020 are used for training and testing. This data set provides the measurement from the dilatometry experiment within the ferrite microstructure of 50 different steel alloys. The left part of Figure 5.16 shows the predictions of the RF regressor on material 2 whereas the right plot demonstrates the GPR predictions on the same data. This plot highlights good prediction of the GPR on material 2 and additionally shows that the real value measurements are within the uncertainty interval.

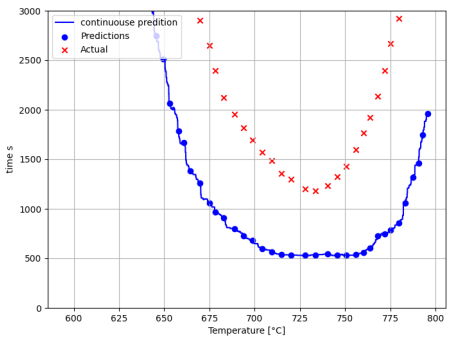


a) RF predictions on material 2 from the ferrite data set.

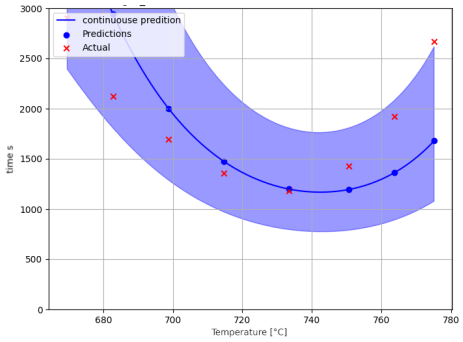


b) GPR predictions on material 2 from the ferrite data set.

Figure 5.16: Material 2 from the ferrite data set predicted by both the GPR and the RF model.

To apply the model to the new data only a few changes are needed, because the input features are similar to the method already implemented (explained in Section 4.2). For example, the descriptor for the supercooling property *Bs* does not exist for ferrite. However, there is a similar measure, which is referred to as the *AT* descriptor. Additionally, to the changed input feature vector, the output vector also differs to the bainitic data set. The bainite target values describe the time when the transformation is completed by 90%, whereas the ferrites target value gives the time after full elongation.

One advantage of the ferrite data set is that it covers the entire c-shape. The bainitic data set is sparser, with mostly just a few data samples for one material. The problem with getting more data samples from one material is that training the GPR, needs to be more efficient or it needs better hardware. The computing needs to be advanced in any way to achieve faster training or faster convergence. Currently the data is down sampled and only every third measurement was taken for training the GPR. This can be observed in Figure 5.16. Additionally, the task allows to neglect measurements above 3000 seconds. This reduces the

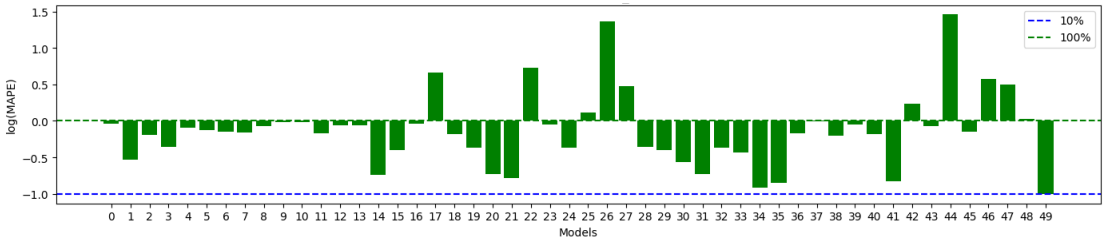


Figure 5.17: Logarithm of MAPE for the leave-one-out splits and the ferrite data set. The green dashed line shows a MAPE of 100% and the blue dashed line shows a MAPE of 10%.

amount of data, but also the quantity of information. Therefore, using the full amount of data is desirable.

Despite the available resources, the RF is trained and tested within the whole data set. The results for the RFs in terms of the MAPE are shown in Figure 5.16. Both ML models make satisfactory predictions for material 2. The GPR has better prediction performance and covers every real value target within the confidence interval except the one at 775°C.

The feature importance for the models is shown in Figure 5.18. For this use-case it is essential, that the iso-thermal holding temperature is of same importance as the *AT* descriptor. In the case of the bainitic steel either the temperature or the additional *Bs* descriptor is crucial for the model. In general, all the elements are of similar significance throughout the different training and test splits. The most important elements for the RF, are Carbon (C), Chrome (Cr), Vanadium (V) and Tungsten (W).

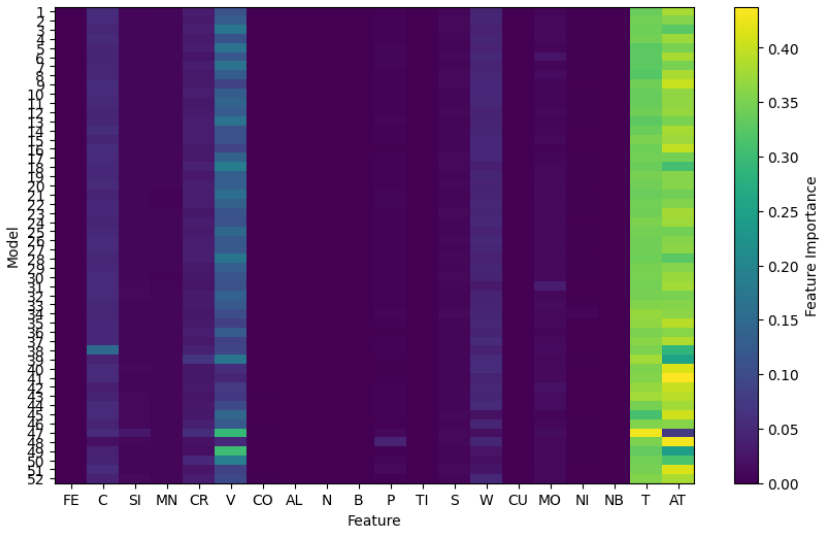


Figure 5.18: Ferrite: feature importance for the RF models trained with leave-one-out method.

## 5.4 Summary

To summarize the results, both models, the GPR and the RF regressor, are effective in most cases. A more robust model can be created by removing certain input features, which is a beneficial approach. This avoids to learn relationships between input and output. However, the same outcome can be achieved by specifying constraints on the hyperparameters. The high-dimensional input vector presents a challenge for the models, particularly in areas with limited data. Extrapolation is challenging due to the potential that small changes in the composite percentages of the reduced feature set, cause totally different measurement behaviour. Both models are neither restricted to the bainitic structure nor to its behaviour. The application of training data from a variety of data sets, including ferrite steel, has shown promising results.

# 6 Conclusion and Future Work

In this thesis, GP and RF are used to model the time (t90%), where the phase fraction of TTT of bainitic steel is 90%. The performance of the prediction depends on the quality of the measurements. Extrapolating to unknown points situated at a considerable distance from the known feature space results in inaccurate estimates. However, a notable advantage of using the GPR is its capacity to provide insight into uncertainty, indicating the confidence level of the estimate. This feature becomes apparent in instances such as Material 15, which contains a percentage of boron, a characteristic does not present in the dataset. Consequently, the model struggles to interpret this unfamiliar information, resulting in estimates of high error. The decision to either trust the estimate or neglect it is indicated by the amount of uncertainty of the GPR. The second model implemented, the RF, does not have any indication like this. Furthermore, it is important to note the sparsity of data points for iso-thermal holding temperatures below 250°C. Such temperatures are rarely encountered in industrial practices, with most data originating from academic institutions and fundamental research. The lack of information in this region presents a significant challenge for the model's perception, making extrapolation difficult. In conclusion, addressing this task proves to be exceedingly challenging for a machine learning model lacking prior knowledge of the physics involved. The scarcity of data further complicates the endeavour. Moreover, the non-linearities inherent in the transformation of the specific microstructure pose a particularly unpredictable challenge, particularly at the extremities of the input feature space. Training a GPR model poses a significant challenge due to the considerable time required for training, especially when using all data and the leave-one-out method. This often results in days of training for a single evaluation. However, future solutions could potentially address this issue by leveraging higher processing power and employing frameworks optimized for GPU utilization. The use of a GPR implementation for scaling up to huge data could be employed to minimize the training effort. Additionally, the t90% problem was introduced as a strategic approach to enhance training efficiency while maintaining the same level of information. To create more robust models and avoid overfitting the model, the number of input features was reduced by neglecting elements which are parts of alloys but do not have a significant effect on the physical behaviour within the measurement. The reduction of the input features is additionally helpful to reduce the parameters to optimise, hence faster training is possible. As more data is collected to train the model,

the issue of complexity becomes more pronounced. While this represents a disadvantage, it is an essential step towards improving prediction accuracy for previously unseen data. Obtaining accurate measurements in terms of quantity and quality is challenging due to the high cost and time-consuming nature of the measurements. The measurement error is significantly high for most measurements, which means that the predictions produced by the model can never be more accurate than the measurements themselves. The model learns and trains with the error, which biases the extrapolation. For the majority of the materials considered, both the RF and GPR models provide satisfactory estimates for the t90% value. While there are slight variations between the two models, particularly for materials with comparable data and iso-thermal holding temperatures, which represent more familiar areas within the feature space, the accuracy of the estimates generally meets the required criteria. Additionally, it is noteworthy that the uncertainty of the GPR indicates that the estimated target falls within the 95% confidence interval provided by the model. One of the key advantages of the GPR model over the RF model is its ability to provide indications of confidence, which are crucial for assessing the reliability of estimates for later use.

ML demonstrates potential for the use within material science. Improving performance can be achieved by multiple ways. One suggestion is to explore additional descriptors that incorporate physics-based principles, providing the model with more comprehensive information to better understand the relationships between alloy behaviours. The supercooling descriptor *Bs* integrated in this thesis is an example of this. As with any machine learning problem, the quality and quantity of training data are crucial. Therefore, efforts to enhance measurement accuracy will lead to more accurate predictions. Furthermore, the number of test samples and materials included in the training set can be increased in order to refine the model's predictions. Moreover, the application of these models and training methodologies to other forms of microstructures could yield insights and results that are unexpected. This could expand the potential applications of the research.

# Bibliography


Ghahramani, Z. (2013). Bayesian non-parametrics and the probabilistic approach to modelling. *Philosophical transactions. Series A, Mathematical, physical, and engineering sciences*, *371*, 20110553. https://doi.org/10.1098/rsta.2011.0553 (cit. on pp. 11, 12).

Huang, X., Wang, H., Xue, W., Ullah, A., Xiang, S., Huang, H., Meng, L., Ma, G., & Zhang, G. (2020). A combined machine learning model for the prediction of time-temperature-transformation diagrams of high-alloy steels. *Journal of Alloys and Compounds*, *823*, 153694. https://doi.org/https://doi.org/10.1016/j.jallcom.2020.153694 (cit. on pp. 6, 41).

Hunkel, M., Surm, H., & Steinbacher, M. (2018). Chapter 3 - dilatometry. In S. Vyazovkin, N. Koga, & C. Schick (Eds.), *Recent advances, techniques and applications* (pp. 103–129, Vol. 6). Elsevier Science B.V. https://doi.org/https://doi.org/10.1016/B978-0-444-64062-8.00019-X (cit. on pp. 3, 4).

Murphy, K. P. (2022). *Probabilistic machine learning: An introduction*. MIT Press. probml.ai (cit. on pp. 15–17).

Rasmussen, C., & Williams, C. (2005). *Gaussian processes for machine learning*. MIT Press. https://books.google.at/books?id=Tr34DwAAQBAJ (cit. on p. 14).

Ronaghan, S. (2019, November). The mathematics of decision trees, random forest and feature importance in scikit-learn and spark. https://towardsdatascience.com/the-mathematics-of-decision-trees-random-forest-and-feature-importance-in-scikit-learn-and-spark-f2861df67e3 (cit. on p. 17).

Yang, Y.-J., Fu, J.-X., Zhao, R.-J., & Wu, Y.-X. (2015). Dilatometric analysis of phase fractions during austenite decomposition in pipeline steel. https://doi.org/10.2991/ic3me-15.2015.380 (cit. on p. 5).